Volume 4 | Number 15 | 21 April 2016 | Pages 5325–5756

Journal of Materials Chemistry A

Materials for energy and sustainability

www.rsc.org/MaterialsA

ISSN 2050-7488

ROYAL SOCIETY OF CHEMISTRY

REVIEW ARTICLE

Hiroaki Benten *et al.*

Recent research progress of polymer donor/polymer acceptor blend solar cells

175 YEARS

Journal of Materials Chemistry A

REVIEW

View Article Online
View Journal | View Issue

Cite this: J. Mater. Chem. A, 2016, 4, 5340

Recent research progress of polymer donor/polymer acceptor blend solar cells

Hiroaki Benten,* Daisuke Mori, Hideo Ohkita and Shinzaburo Ito

Received 30th December 2015
Accepted 25th February 2016

DOI: 10.1039/c5ta10759h

www.rsc.org/MaterialsA

Polymer/polymer blend solar cells based on a blend of two types of conjugated polymers acting as an electron donor (hole transport) and acceptor (electron transport) have recently attracted considerable attention, because they have numerous potential advantages over conventional polymer/fullerene blend solar cells. The highest power conversion efficiency (PCE) was slightly above 2% five years ago, whereas PCEs of beyond 8% are the state-of-the-art today, and the efficiency gap between polymer/polymer and polymer/fullerene systems has closed very rapidly. In this review, we provide an overview of recent progress towards the performance enhancement of polymer/polymer blend solar cells. In addition, we discuss the future outlook and challenges regarding PCEs beyond 10%.

1. Introduction

The continued increase in energy consumption worldwide necessitates the development of a global energy supply based on limitless resources, which should also generate less greenhouse gases than fossil-fuel-based energy sources. In this regard, the exploitation of photovoltaic energy is a promising approach that has the potential to solve the energy supply problems emerging in the foreseeable future. In particular, organic photovoltaics (OPVs) have gained increasing attention as an inexpensive source of renewable energy owing to their unique advantages, which include high throughput and large-area production with low-cost printing processes.[1,2] Among the various OPVs, the most widely studied solar cells consist of a bulk-heterojunction (BHJ) structure in which a conjugated polymer is mixed with a low-molecular-weight fullerene derivative.[3–5] In these systems, the conjugated polymer acts as an electron donor and the fullerene derivative acts as an electron acceptor. The power conversion efficiency (PCE) of polymer/fullerene blend solar cells has been enhanced significantly over the past two decades, and exceeds 10% in single-junction cells.[6–9]

On the other hand, polymer/polymer blend solar cells that utilize conjugated polymers as both an electron donor and an electron acceptor have recently attracted considerable attention, because they have numerous potential advantages over conventional polymer/fullerene blend solar cells.[10–13] In

Department of Polymer Chemistry, Graduate School of Engineering, Kyoto University, Katsura, Nishikyo, Kyoto 615-8510, Japan. E-mail: benten@photo.polym.kyoto-u.ac.jp; Fax: +81 75 383 2617; Tel: +81 75 383 2614

Hiroaki Benten is an Assistant Professor of the Department of Polymer Chemistry at Kyoto University. He obtained his PhD from Kyoto University in 2005. From 2006 to 2008, he worked as a JSPS postdoctoral fellow at the Max-Planck Institute for Polymer Research (Mainz), in the laboratory operated by Professor Knoll. He became an Assistant Professor in 2008. In 2013, he worked as an academic visitor under Professor Ginger at the University of Washington. His current research interests are nanoscale morphology, photophysical processes, and functions of conjugated polymer-based materials.

Mori Daisuke has been a materials researcher at Sony Corporation since April 2015. He received his BS (2010) and MS (2012) degree from the Department of Polymer Chemistry at Kyoto University. In 2015, he received his PhD from the Department of Polymer Chemistry at Kyoto University, under the supervision of Prof. Shinzaburo Ito. His thesis title is "Development of Polymer Blend Solar Cells Composed of Conjugated Donor and Acceptor Polymers."

particular, the flexible molecular design of not only the donor, but also the acceptor material provides extensive scope for tuning the optical, electronic, morphological, and mechanical properties of the blended films. For instance, conjugated polymers have high absorption coefficients (α) in the visible and near-infrared (IR) spectral regions. Therefore, polymer/polymer blends can harvest a large fraction of solar light, leading to a large short-circuit photocurrent density (J_{SC}). Furthermore, the adjustment of the highest occupied molecular orbital (HOMO) and lowest unoccupied molecular orbital (LUMO) levels of the donor and acceptor polymers allows the open-circuit voltage (V_{OC}) to increase above 1 V. In addition, the formation of a phase-separated interpenetrating polymer network offers a continuous pathway for charge carrier transport, for wide ranges of donor and acceptor material blending ratios, leading to a high fill factor (FF). Finally, all-polymer blends yield superior thin-film formation properties, including flexibility and mechanical robustness, which are extremely beneficial for the large-scale production of solar cell modules *via* solution processes.[14]

As a result of their many advantages, various polymer acceptors have been considered as an alternative to fullerene derivatives such as [6,6]-phenyl-C_{61}-butyric acid methyl ester (PCBM); however, the majority of these polymers have exhibited significantly lower electron mobility (μ_e) than the fullerene derivatives. Moreover, the BHJ phase-separated structures are typically larger in polymer/polymer blends than in polymer/fullerene blends, resulting in lower charge generation efficiency. Consequently, despite the attractive features of these materials, the development of polymer/polymer blend solar cells has lagged behind that of their polymer/fullerene counterparts, with the PCEs of the former being approximately 2% until 2012. Very recently, however, significant strides have been made towards enhancing the PCEs of polymer/polymer blend solar cells, owing to considerable efforts expended on developing low-bandgap polymer acceptors with both high-μ_e and high electron affinity (similar to those of fullerene derivatives) and, also, attempts to optimize the blend morphology.

In this review, we briefly present the fundamental characteristics of polymer/polymer blend solar cells, provide an overview of recent progress towards enhancing their photovoltaic performance, and discuss research on the optimal blend morphology and free charge-carrier generation at donor/acceptor heterojunctions of polymer blends. Finally, we discuss the future outlook and challenges regarding the achievement of PCEs of 10% and higher.

2. Operation of polymer/polymer blend solar cells

2.1 Blend morphology for BHJs

Blends of two different polymers are likely to form a large phase-separated structure; this is an inherent characteristic of polymers with a long main chain. According to the Flory–Huggins theory,[15,16] the change in the Gibbs free energy when two polymers are mixed (ΔG_{mix}) can be derived as follows:

$$\frac{\Delta G_{mix}}{nk_BT} = \frac{\varphi_A}{N_A}\ln(\varphi_A) + \frac{\varphi_B}{N_B}\ln(\varphi_B) + \chi\varphi_A\varphi_B \quad (1)$$

where $\varphi_{A/B}$ is the volume fraction of polymer A/B (with $\varphi_A + \varphi_B = 1$), $N_{A/B}$ is the degree of polymerization of polymer A/B, n is the total number of segments, k_B is the Boltzmann constant, T is the temperature, and χ is the Flory–Huggins interaction parameter. The first two terms on the right-hand side of eqn (1) represent the entropy component, whereas the final term represents the enthalpy contribution. For polymer/polymer blends, the entropy gain is reduced by a factor of $N_{A/B}$. That is, when long polymer chains are mixed, they do not gain sufficient entropy to yield a negative ΔG_{mix}. In addition, in the enthalpy component, χ is an interaction parameter between two polymers, where

Hideo Ohkita is an Associate Professor of the Department of Polymer Chemistry at Kyoto University. He obtained his PhD from Kyoto University in 1997. He became an Assistant Professor in 1997 and was promoted to Associate Professor in 2006. From 2005 to 2006, he worked as an academic visitor with Professor Durrant at Imperial College London. From 2009 to 2015, he was concurrently a PRESTO researcher, Japan Science and Technology Agency (JST). His research interests include the study of photophysics and photochemistry in polymer systems. His current research focuses on the spectroscopic approach to polymer solar cells.

Shinzaburo Ito is a Professor of the Department of Polymer Chemistry at Kyoto University. He obtained his PhD in Engineering from Kyoto University in 1981. He was appointed as a Research Instructor at Kyoto University in 1979, and worked as a guest scientist at the Max-Planck Institute for Polymer Research (Mainz) from 1991 to 1992, in the laboratory operated by Professor Knoll. He was also a visiting research fellow at RIKEN (Wako) from 1993 to 1999. He was promoted to Associate Professor in 1994 and to Professor of the Department of Polymer Chemistry, Kyoto University, in 1999. His research interests encompass polymer nanostructure, polymer photophysics and photochemistry, and ultrathin films and their optical and electrical properties.

a small value of χ is required in order to obtain a well-mixed structure. The entropy terms are negative but small, and the enthalpy of mixing is likely to be positive. Consequently, polymer/polymer blends tend to phase-separate on a micrometer scale, which is undesirable with regard to the photocurrent generation, because the majority of the excitons cannot reach the donor/acceptor heterojunction for charge generation.[17–21] For polymer/polymer blends, it is, therefore, critically important to suppress phase separation.

2.2 Photovoltaic conversion mechanism

Fig. 1 is a schematic illustration of the working mechanism of polymer/polymer blend solar cells. Photovoltaic conversion processes can be divided into several sequential processes: (1) absorption of an incident photon by the constituent polymers, leading to the formation of polymer singlet excitons; (2) diffusion of the excitons to a donor/acceptor domain interface (heterojunction); (3) charge transfer at the interface driven by either the LUMO–LUMO or HOMO–HOMO energy offsets of the donor and acceptor polymers, along with dissociation of the interfacial charge transfer state into free charge carriers; and (4) transport of the free charge carriers to the anode and cathode through bicontinuous networks of donor (hole-transporting) and acceptor (electron-transporting) polymers.[10,11,22–25] As a result, the incident photon energy can be converted into electricity and a direct current is supplied to an external circuit. Among these conversion processes, exciton diffusion to the domain interface is particularly important, because the diffusion length of a polymer singlet exciton (L_D) is typically as short as only 10 nm.[17–21] Therefore, excitons generated at a distance of more than 10 nm from the donor/acceptor domain interface cannot contribute to the photocurrent generation. In addition, even if charge carriers are converted from the excitons, the charges generated in isolated polymer domains cannot be transported by the electrodes. The overall photovoltaic performance is, thus, significantly affected by the morphological characteristics of the blends, such as the domain size, domain composition (purity), and domain connectivity. The ideal BHJ structure for efficient charge generation and transport is considered to be a nanostructured blend based on bicontinuous interpenetrating networks of pure donor and acceptor domains with a characteristic spacing length of ~10 nm, which is comparable to L_D.

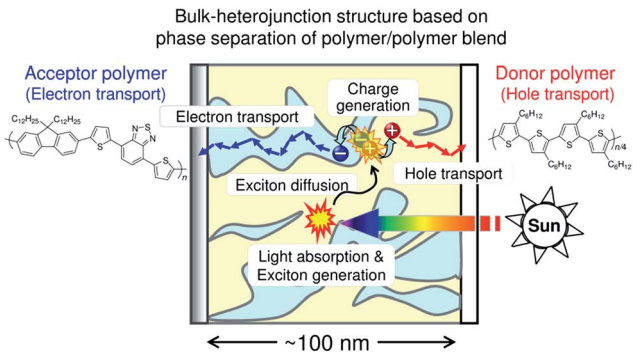

Fig. 1 Photovoltaic conversion processes in polymer/polymer blend solar cells: (1) exciton generation *via* photon absorption; (2) exciton diffusion at a donor/acceptor interface; (3) charge transfer at the interface and charge dissociation into free charge carriers; and (4) charge transport to each electrode.

3. Efficiency enhancement of polymer/polymer blend solar cells over the past decade

Here, we describe the research progress with regard to the efficiency enhancement of polymer/polymer blend solar cells over the past decade. The solar cell performances of the devices discussed in this section are summarized in Table 1. Fig. 2 shows selected PCEs reported for polymer/polymer blend solar cells over the past 10 years. Although the PCE remained at approximately 2% for a long period of time, it increased rapidly from 2012 onwards, and PCEs of over 8% have already been reported. In Fig. 3, these PCEs are plotted as functions of the corresponding device parameters: J_{SC}, V_{OC}, and FF. Among the device parameters, an increase in J_{SC} is most strongly correlated with an increase in PCE (see the broken line in Fig. 3a). As indicated by the various symbols in Fig. 2 and 3, the enhancement of polymer/polymer blend solar cell efficiency can be discussed by considering the development of polymer acceptors.

In the earliest development stage, cyano-substituted phenylenevinylene (CN-PPV) polymers were most widely used as polymer acceptors. Then, fluorene and benzothiadiazole (BT)-based copolymers were considered as electron acceptors. Both CN-PPV derivatives (the diamonds in Fig. 2 and 3) and fluorene and BT-based copolymers (the triangles in Fig. 2 and 3) yield a high V_{OC} (>1 V), because of their relatively shallow LUMO energy levels. However, the J_{SC} and FF are low, because the light absorption ability of these polymer acceptors is limited to the visible region and, also, their μ_e values are relatively low ($\sim 10^{-5}$ cm^2 V^{-1} s^{-1}). Consequently, the PCEs of most devices based on these acceptors remained at less than 2% for a long period of time.

Subsequently, copolymers based on two kinds of rylene diimides, perylene diimide (PDI; squares in Fig. 2 and 3) and naphthalene diimide (NDI; circles and stars in Fig. 2 and 3) were synthesized as polymer acceptors that exhibit high μ_e, high electron affinities similar to those of fullerenes, and absorption bands from the visible to the near-IR region. From 2012 onwards, several kinds of NDI-based polymers were combined with low-bandgap polymer donors to enhance the light absorptivity of the photoactive blend layer in the near-IR region, leading to an increase in J_{SC} and considerable improvement in the PCE. The chemical structures of polymer acceptors employed in polymer/polymer blend solar cells are shown in Fig. 4–7, and those of polymer donors are illustrated in Fig. 8.

3.1 Cyanated phenylenevinylene-based polymer acceptors

Halls *et al.* reported the pioneering work on polymer/polymer blend solar cells in 1995.[26] They employed a polymer blend film of two soluble poly(*p*-phenylenevinylene) (PPV) derivatives, poly[2-methoxy-5-(2′-ethyl)-hexyloxy-*p*-phenylenevinylene] (MEH-PPV) and

Table 1 Photovoltaic parameters of polymer/polymer blend solar cells

	Donor	Acceptor	D : A blend ratio (w/w)	Thickness (nm)	PCE (%)	J_{SC} (mA cm^{-2})	V_{OC} (V)	FF	EQE$_{max}$ (%)	μ_h (cm^2 V^{-1} s^{-1})	μ_e (cm^2 V^{-1} s^{-1})	Device type	Ref.
2015	J51	P(NDI2OD-T2)	2 : 1	120	8.27	14.18	0.83	0.702	75	2.50×10^{-4}	2.16×10^{-4}	Normal	77
2015	PTB7-Th	PNDIS-HD	1 : 1	115	7.73	18.8	0.81	0.51	85	3.11×10^{-4}	7.25×10^{-3}	Inverted	76
2015	PTB7-Th	P(NDI2DT-FT2)	1 : 1	110	6.71	13.53	0.81	0.62	66	5.50×10^{-4}	4.90×10^{-4}	Inverted	75
2015	PBDTTTPD	PNDIT-HD	1.3 : 1	130	6.64	11.22	1.06	0.56	70	2.84×10^{-5}	1.55×10^{-5}	Normal	14
2015	PBDTTT-C-T	30PDI	1 : 1	90	6.29	18.55	0.79	0.45	91	2.60×10^{-3}	1.00×10^{-3}	Inverted	74
2015	PTB7-Th	PNDIT-HD	1.3 : 1	90–100	5.96	13.46	0.79	0.56	70	2.80×10^{-4}	8.40×10^{-4}	Inverted	73
2015	PBDTBDD-T	P(NDI2OD-T2)	1 : 1	85–90	5.8	11.7	0.87	0.575	55	1.10×10^{-3}	—	Normal	72
2015	PTB7-Th	P(NDI2OD-T2)	1 : 1	100	5.2	13.9	0.74	0.49	60	—	—	Normal	62
2015	PPDT2FBT	P(NDI2OD-T2)	1 : 0.7	90–100	5.1	11.9	0.85	0.51	59	2.00×10^{-4}	4.70×10^{-5}	Normal	71
2015	PTP8	P(NDI2OD-T2)	2 : 1	92	4.35	8.43	0.978	0.528	46–47	4.78×10^{-5}	8.48×10^{-5}	Normal	70
2015	PTQ1	P(NDI2OD-T2)	7 : 3	100	3.9	8.02	0.85	0.57	45	6.27×10^{-5}	1.02×10^{-4}	Normal	62
2015	PBDTTT-C-T	PNDIBTOC8	6 : 4	—	3.14	7.65	0.9	0.456	33	4.20×10^{-4}	2.80×10^{-4}	Normal	69
2015	PTB7-Th	PQP	1 : 1	—	3.08	7.72	0.7	0.57	38	1.34×10^{-4}	1.75×10^{-7}	Normal	68
2015	P3HT	PDPP2TzT	2 : 1	115	3	7.8	0.64	0.61	30	—	—	Inverted	67
2015	PBDTBDD-T	PBDTNDI-T	1.5 : 1	—	2.88	5.62	0.86	0.596	43	—	—	Normal	66
2015	PTB7	PCPDT-PDI	1 : 1	80–90	2.13	7.25	0.7	0.42	34	1.30×10^{-4}	9.80×10^{-6}	Normal	63
2015	PBDTTT-C-T	C3	1 : 1	—	1.85	4.75	0.79	0.49	19.6	1.80×10^{-4}	1.00×10^{-4}	Normal	65
2015	P3HT	PPDI25-*co*-NDI75	3 : 1	—	1.54	3.62	0.68	0.624	22.5	3.70×10^{-4}	3.00×10^{-5}	Normal	64
2015	PTB7	PCPDT-NDI	1 : 1	80–90	1.12	3.85	0.74	0.39	—	—	—	Normal	63
2015	P3HT	P(NDI2OD-T2)	1 : 1	100	0.65	2.53	0.49	0.53	19	—	—	Normal	62
2014	PTB7-Th	P(NDI2OD-T2)	1 : 1	100	5.73	13	0.794	0.556	60	3.40×10^{-4}	3.60×10^{-4}	Normal	61
2014	NT	P(NDI2OD-T2)	1 : 1	90	5	11.5	0.77	0.56	52–53	2.50×10^{-4}	6.90×10^{-4}	Inverted	60
2014	PSEHTT	PNDIS-HD	1 : 1	70–80	4.81	10.47	0.76	0.6	61.3	5.40×10^{-4}	2.60×10^{-4}	Inverted	59
2014	PTB7-Th	P(NDI2OD-T2)	1.3 : 1	110–120	4.6	10.61	0.821	0.53	53.6	4.20×10^{-4}	6.70×10^{-6}	Inverted	58
2014	Pil-2T-PS5	P(TP)	—	93	4.21	8.77	1.04	0.46	46	2.00×10^{-4}	2.00×10^{-5}	Inverted	57
2014	PBDTTT-C-T	P(PDI-DTT)	1 : 1	60–85	3.45	8.55	0.752	0.515	43	2.64×10^{-4}	3.37×10^{-5}	Normal	56
2014	PTB7	P(NDI2OD-T2)	1 : 1.5	120	2.66	6.28	0.799	0.53	27	3.90×10^{-6}	4.80×10^{-4}	Inverted	55
2014	P3HT	P(NDI2OD-T2)	1 : 0.75	310	—	—	—	0.67	—	1.20×10^{-3}	4.00×10^{-3}	Normal	54
2014	P3HT	P(NDI2OD-T2)	1 : 0.75	310	—	—	—	0.5	—	2.00×10^{-3}	7.00×10^{-3}	Normal	54
2014	P3HT	F8TBT	1 : 1	80	1.87	3.29	1.35	0.42	20	—	—	Normal	53
2014	P3HT	PFDTBT-OC6	1 : 2	80	1.80	2.93	1.36	0.45	22	—	—	Normal	52
2013	PTQ1	P(NDI2OD-T2)	7 : 3	85	4.1	8.85	0.84	0.55	50	1.13×10^{-5}	2.58×10^{-3}	Normal	51
2013	TTV7	PC-NDI	2 : 1	80–90	3.68	7.71	0.88	0.54	40	3.70×10^{-4}	1.70×10^{-4}	Normal	50
2013	PSEHTT	PNDIS-HD	1 : 1	70	3.26	7.78	0.76	0.55	47	2.00×10^{-4}	1.00×10^{-4}	Inverted	49
2013	P3HT	PDI-diTh	1 : 1.5	120–130	2.17	7.65	0.52	0.55	40	—	—	Inverted	48
2013	PTB7	P(NDI2OD-T2)	1 : 1	70	1.1	3.4	0.62	0.39	—	—	—	Normal	47
2012	P3HT	PF12TBT	1 : 1	60	2.7	3.88	1.26	0.55	—	—	—	Normal	46
2012	P3HT	PF-NDI	2 : 1	—	1.63	3.63	0.68	0.66	30	—	—	Normal	45
2012	P3HT	P(NDI2OD-T2)	1 : 0.75	275	1.4	3.77	0.56	0.65	22	—	—	Normal	44
2012	P3HT	P(NDI-TCPDTT)	1 : 1.5	410	1.1	2.43	0.63	0.7	16	—	—	Normal	44
2012	P3HT	PNDIBS	1 : 3	—	0.88	3.79	0.53	0.44	19	—	—	Normal	43
2011	PT1	PC-PDI	2 : 1	—	2.23	6.35	0.7	0.5	43	—	—	Normal	42
2011	P3HT	PF12TBT	1 : 1	70	2	3.94	1.19	0.42	27	—	—	Normal	41
2011	POPT	CN-PPV	—	—	2	5.44	1.06	0.35	—	—	—	Normal	40
2011	P3HT	P(NDI2OD-T2)	1 : 2	—	0.62	2.39	0.48	0.54	15.8	—	—	Normal	39

Table 1 (*Contd.*)

	Donor	Acceptor	D : A blend ratio (w/w)	Thickness (nm)	PCE (%)	J_{SC} (mA cm^{-2})	V_{OC} (V)	FF	EQE_{max} (%)	μ_h (cm^2 V^{-1} s^{-1})	μ_e (cm^2 V^{-1} s^{-1})	Device type	Ref.
2011	P3HT	P(NDI2OD-T2)	1 : 2	—	0.16	0.48	0.50	0.67	—	—	—	Normal	39
2010	P3HT	F8TBT	1 : 1	75–80	1.85	3.3	1.14	0.49	26.1	—	—	Inverted	38
2009	PPHT	PDI-PPV copolymer	1 : 1	—	2.32	2.98	0.6	0.39	—	—	—	Normal	37
2009	POPT	CN-PPV	—	—	2	—	—	—	—	—	—	Normal	36
2009	PTZV-PT	DOCN-PPV	1 : 1	60	0.8	3.14	0.85	0.288	25	—	—	Normal	35
2008	Polythiophene derivative 2	P(PDI-DTT) derivative	3 : 1	60	1.48	5.02	0.69	0.43	37	—	—	Normal	34
2007	P3HT	F8TBT	1 : 1	70	1.8	4	1.25	0.45	26	—	—	Normal	33
2007	Polythiophene derivative 1	P(PDI-DTT)	1 : 1	—	1	4.2	0.63	0.39	44	—	—	Normal	32
2006	MDMO-PPV	PF1CVTP	—	40–50	1.5	3	1.4	0.37	40	—	—	Normal	31
2005	M3EH-PPV	CN-ether-PPV	1 : 1	55	1.7	3.57	1.36	0.354	31	—	—	Normal	30
2004	M3EH-PPV	CN-ether-PPV	1 : 1	60	1.0	3.2	1.0	0.25	—	—	—	Normal	29
2004	M3EH-PPV	CN-ether-PPV	1 : 1	45	0.75	3.3	0.65	0.35	23.5	—	—	Inverted	29
1998	POPT	MEH-CN-PPV	—	—	1.9	—	—	—	29	—	—	Normal	28

Fig. 2 Efficiency enhancement of polymer/polymer blend solar cells based on different polymer acceptors: cyanated phenylenevinylene-based polymers (diamonds); fluorene and BT-based polymers (triangles); thiazole-bridged diketopyrrolopyrrole-polymer (inverted triangle);[67] PDI-based polymers (squares); and NDI-based polymers (circles).

cyano-PPV (CN-PPV), as a photoactive layer. The phase-separated structures were as small as 10–100 nm, as observed in transmission electron microscopy images, which was consistent with efficient photoluminescence (PL) quenching in the blend. As a result, the polymer blend device exhibited a photoresponse corresponding to polymer absorption. In the same year, Yu *et al.* reported a similar study.[27] The polymer combination they employed (MEH-PPV and MEH-CN-PPV) was almost identical to that reported by Halls *et al.*, although the CN-PPV side chain differed slightly. The polymer blend device exhibited an energy conversion efficiency of 0.9%, which was 20 times larger than that of pure MEH-PPV and ~100 times larger than that of pure MEH-CN-PPV. (Note that the conversion efficiency was measured at an intensity of $\sim 10^{-6}$ W cm^{-2}.) These findings demonstrate that blending of conjugated donor and acceptor polymers can provide not only donor/acceptor interfaces for the generation of charge carriers, but also interpenetrating networks to transport charge carriers to each electrode.

A decade after these pioneering studies, a PCE exceeding 1% was obtained for polymer blend solar cells, with some effort. In 2005, Kietzke *et al.* reported polymer blend solar cells based on poly[2,5-dimethoxy-1,4-phenylene-1,2-ethenylene-2-methoxy-5-(2-ethylhexyloxy)-(1,4-phenylene-1,2-ethenylene)] (M3EH-PPV) and poly[oxa-1,4-phenylene-1,2-(1-cyano)ethylene-2,5-dioctyloxy-1,4-phenylene-1,2-(2-cyano)ethylene-1,4-phenylene] (CN-ether-PPV).[30] These devices exhibited a PCE of 1.7% under white light illumination at 100 mW cm^{-2}. Kietzke *et al.* attributed this high efficiency to the formation of a vertically graded composition structure in the blended layer, as a result of the different solubilities of the M3EH-PPV and CN-ether-PPV in chlorobenzene. In 2006, Koetse *et al.* reported polymer/polymer blend solar cells based on poly[2-methoxy-5-(3,7-dimethyloctyloxy)-1,4-phenylenevinylene] (MDMO-PPV) and poly[9,9-dioctylfluorene-2,7-diyl-*alt*-1,4-bis[2-(5-thienyl)-1-cyanovinyl]-2-methoxy-5-(3,7-dimethyloctyloxy)benzene] (PF1CVTP).[31] For a device prepared with an additional thin layer (~5 nm) of the acceptor material between the photoactive blend layer and the electron-collecting electrode, the highest PCE of 1.5% was obtained under AM 1.5G illumination at 100 mW cm^{-2}. Further, in 2009, Fréchet *et al.* reported polymer/polymer bilayer solar cells based on poly[3-(4-*n*-octyl)-phenylthiophene] (POPT) and MEH-CN-PPV.[36] These

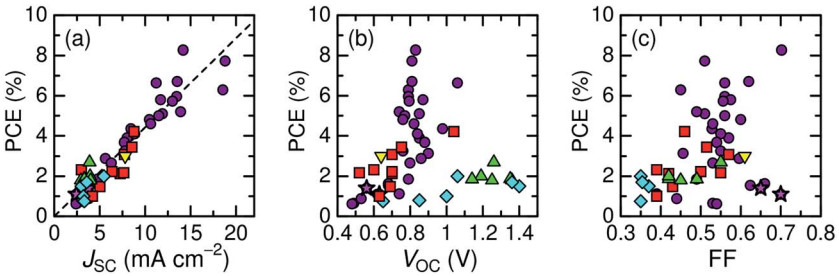

Fig. 3 Power conversion efficiencies of polymer/polymer blend solar cells with corresponding device parameters: (a) J_{SC}; (b) V_{OC}; and (c) FF. Each symbol represents a different polymer acceptor: cyanated phenylenevinylene-based polymers (diamonds); fluorene and BT-based polymers (triangles); thiazole-bridged diketopyrrolopyrrole-polymer (inverted triangle);[67] PDI-based polymers (squares); and NDI-based polymers (circles and stars).

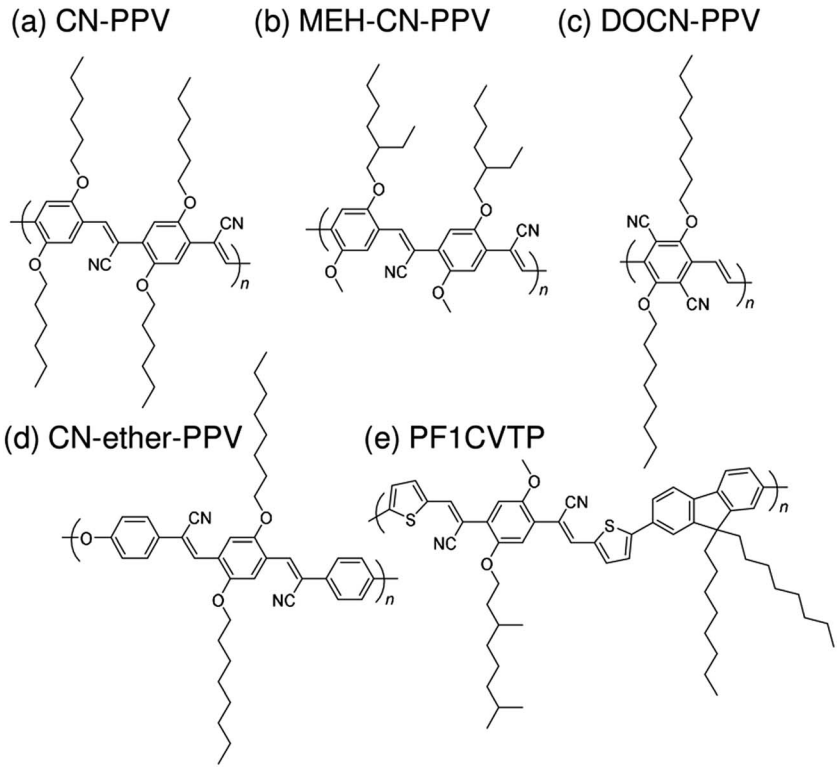

Fig. 4 Chemical structures of cyanated phenylenevinylene-based polymer acceptors: (a) CN-PPV; (b) MEH-CN-PPV; (c) DOCN-PPV; (d) CN-ether-PPV; and (e) PF1CVTP.

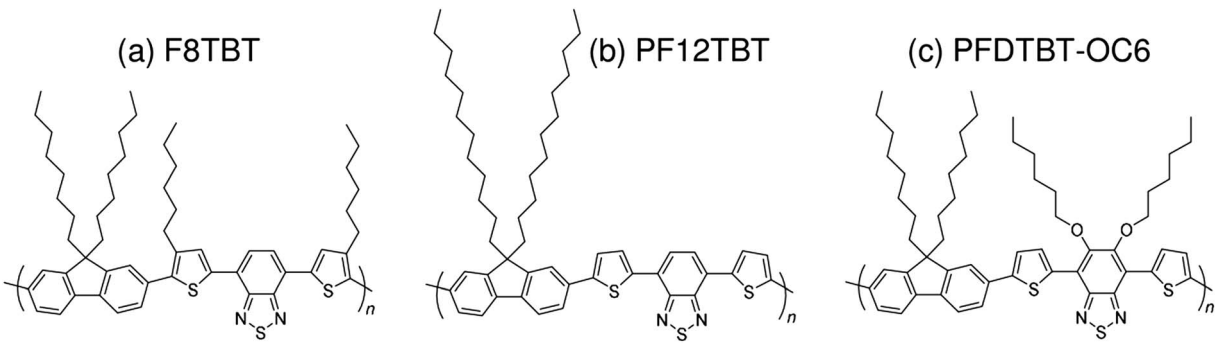

Fig. 5 Chemical structures of fluorene and BT-based polymer acceptors: (a) F8TBT; (b) PF12TBT; and (c) PFDTBT-OC6.

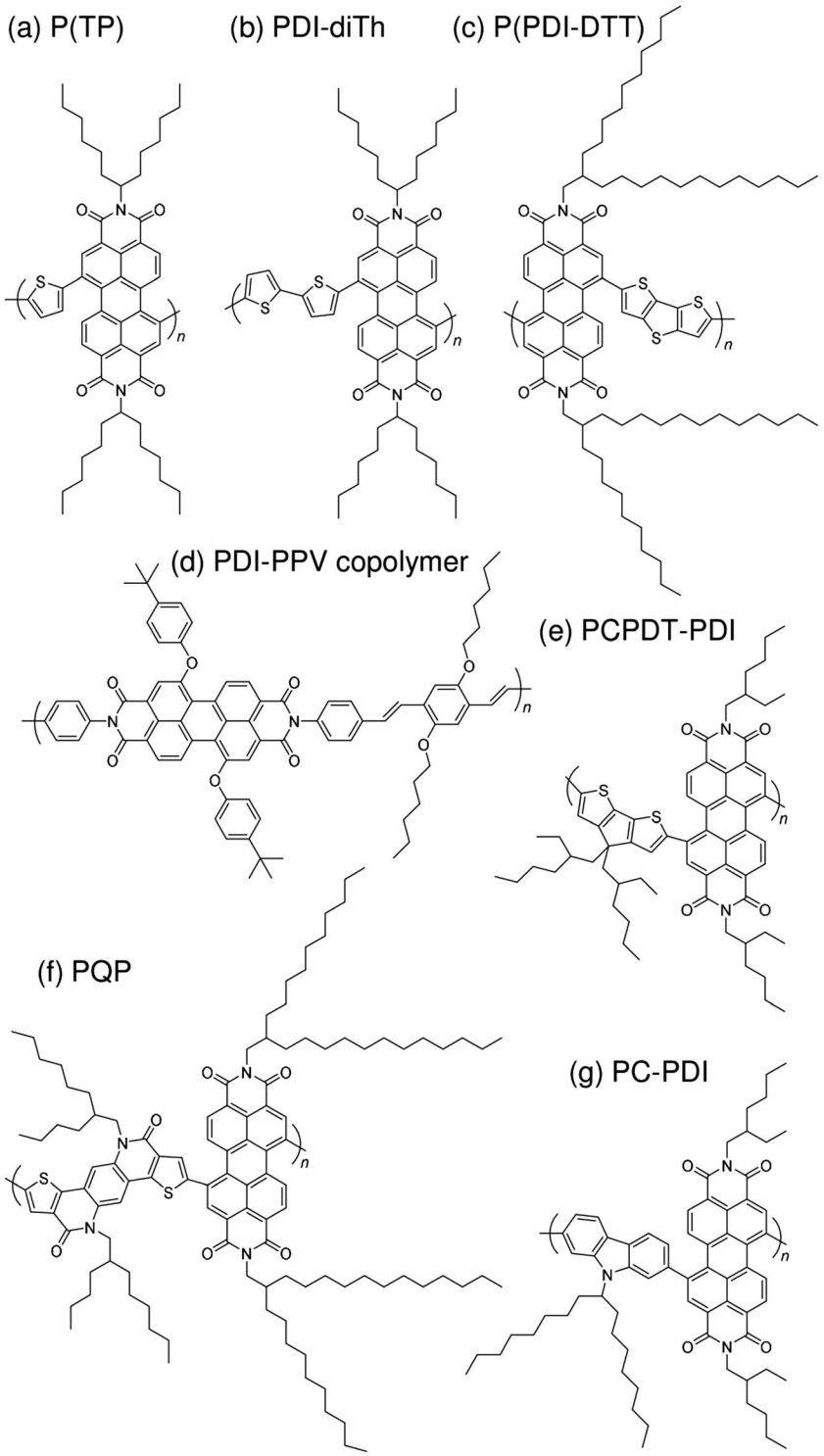

Fig. 6 Chemical structures of PDI-based polymer acceptors: (a) P(TP); (b) PDI-diTh; (c) P(PDI-DTT); (d) PDI-PPV copolymer; (e) PCPDT-PDI; (f) PQP; and (g) PC-PDI.

researchers synthesized POPT using a modified Grignard metathesis (GRIM) procedure. Because of the high number-average molecular weight (M_n) and regioregularity of POPT, MEH-CN-PPV can be spin-coated directly on top of a GRIM POPT film to yield bilayer POPT/MEH-CN-PPV devices with a PCE of 2.0%.

3.2 Fluorene and benzothiadiazole (BT)-based polymer acceptors

In 2007, McNeil *et al.* reported a PCE of 1.8% for polymer/polymer blend solar cells based on regioregular poly(3-hexylthiophene) (P3HT) and poly[9,9-dioctylfluorene-2,7-diyl-*alt*-[4,7-bis(3-hexylthien-5-yl)-2,1,3-benzothiadiazole]-2′,2″-diyl] (F8TBT).[33] Later, in 2010, Huck *et al.*

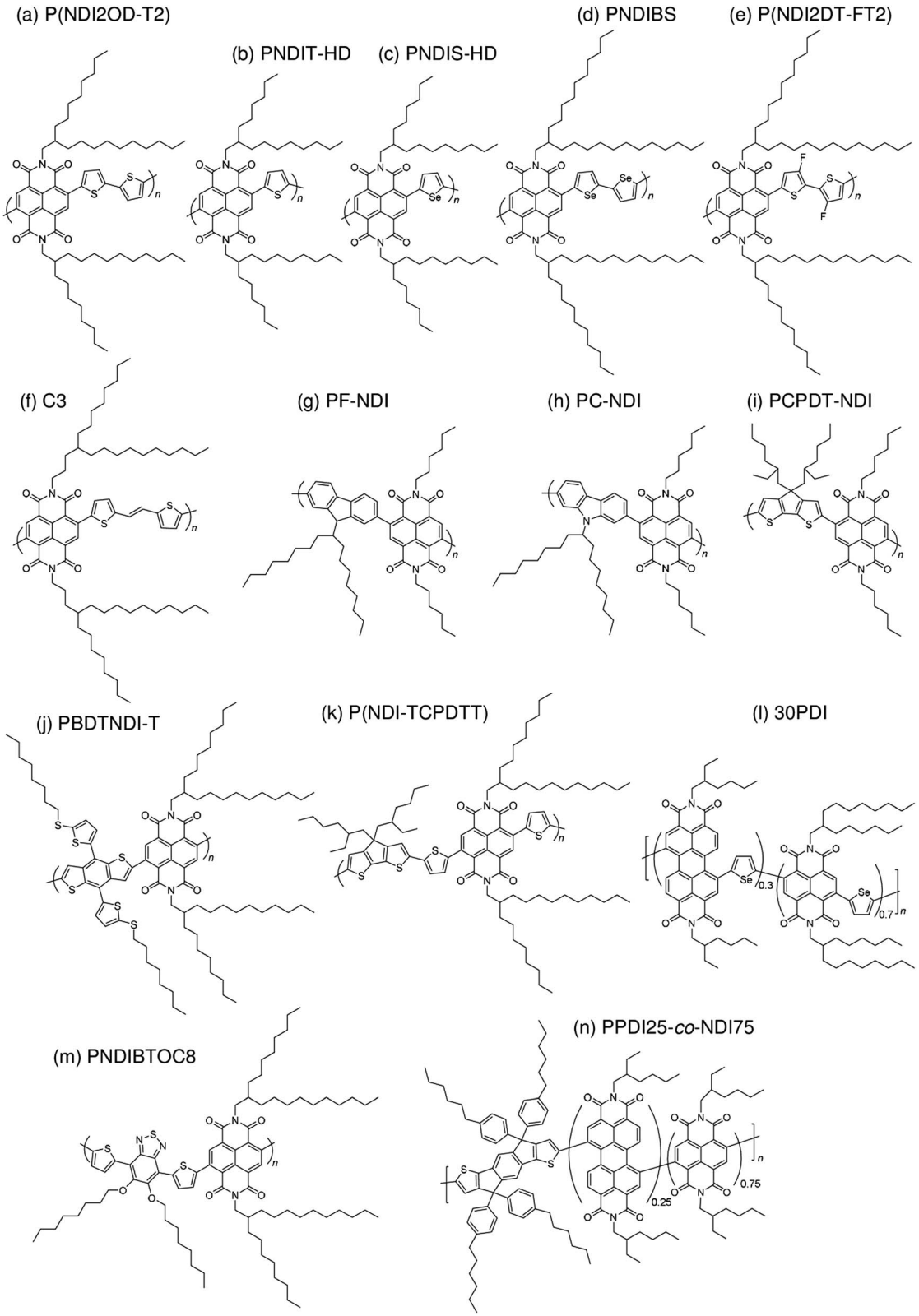

Fig. 7 Chemical structures of NDI-based polymer acceptors: (a) P(NDI2OD-T2); (b) PNDIT-HD; (c) PNDIS-HD; (d) PNDIBS; (e) P(NDI2DT-FT2); (f) C3; (g) PF-NDI; (h) PC-NDI; (i) PCPDT-NDI; (j) PBDTNDI-T; (k) P(NDI-TCPDTT); (l) 30PDI; (m) PNDIBTOC8; and (n) PPDI25-*co*-NDI75.

reported nanopatterned P3HT/F8TBT solar cells fabricated using a nanoimprinting technique.[38] The nanopatterned polymer solar cells exhibited a PCE of 1.85%, with a pattern size of 25 nm on a 50 nm pitch, which is comparable to L_D. Moreover, in 2014, Li *et al.* reported solar cells made from blends of P3HT-nanowires and F8TBT, for which a PCE of 1.87% was achieved.[53]

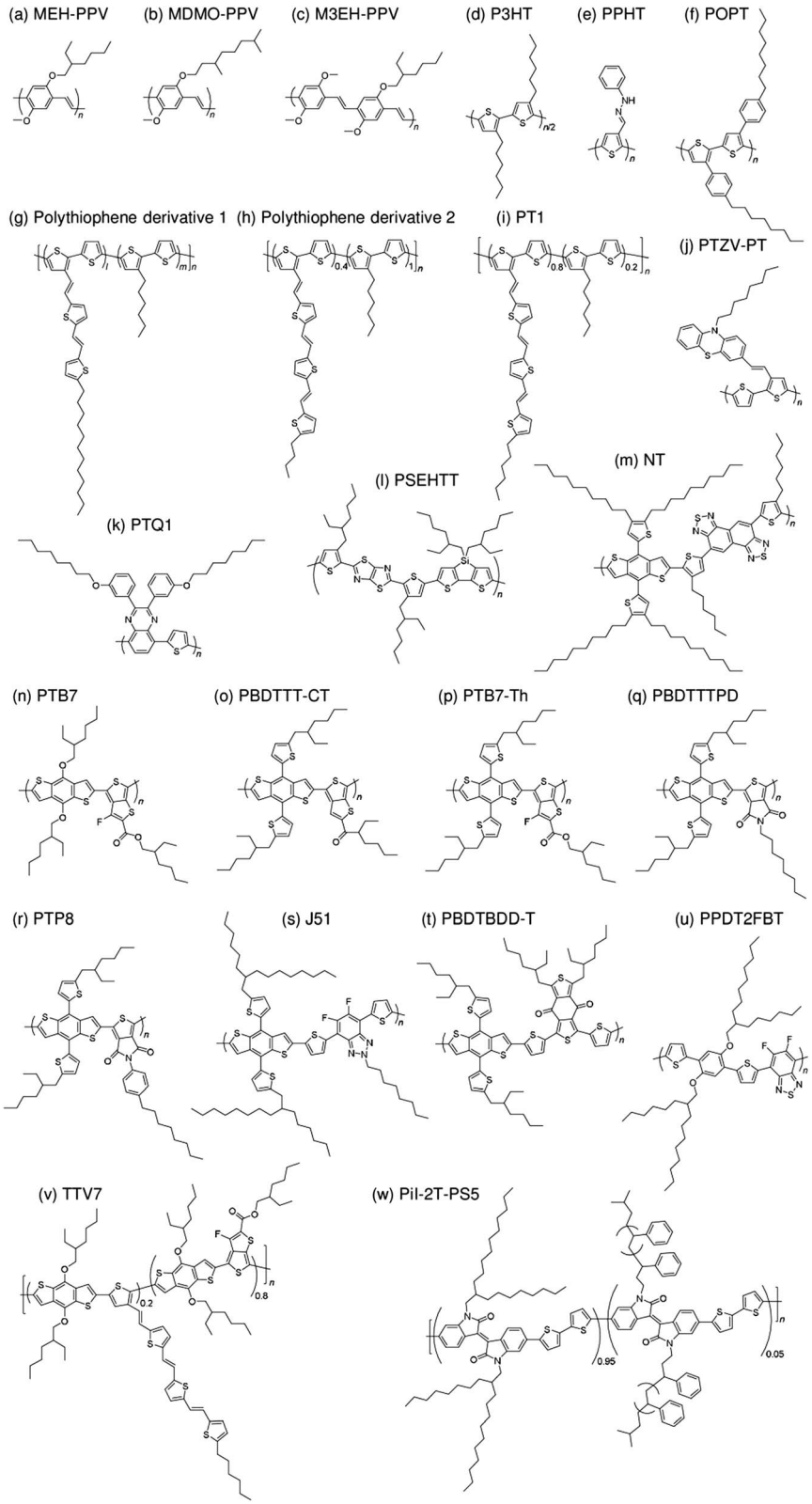

Fig. 8 Chemical structures of polymer donors employed in polymer/polymer solar cells: (a) MEH-PPV; (b) MDMO-PPV; (c) M3EH-PPV; (d) P3HT; (e) PPHT; (f) POPT; (g) polythiophene derivative 1; (h) polythiophene derivative 2; (i) PT1; (j) PTZV-PT; (k) PTQ1; (l) PSEHTT; (m) NT; (n) PTB7; (o) PBDTTT-CT; (p) PTB7-Th; (q) PBDTTTPD; (r) PTP8; (s) J51; (t) PBDTBDD-T; (u) PPDT2FBT; (v) TTV7; and (w) PiI-2T-PS5.

In 2011, Ito *et al.* reported a PCE of 2.0% for polymer/polymer blend solar cells based on P3HT and poly[2,7-(9,9-didodecylfluorene)-*alt*-5,5-[4′,7′-bis(2-thienyl)-2′,1′,3′-benzothiadiazole]] (PF12TBT).[41] These researchers further improved the PCE of P3HT/PF12TBT solar cells to 2.7% through the use of PF12TBT with a high weight-average molecular weight (M_w) of 78 000 g mol^{-1}.[46] In addition, in 2014, Xie *et al.* reported a PCE of 1.80% for polymer/polymer blend solar cells based on P3HT and poly [2,7-(9,9′-octyl-fluorene)-*alt*-5,5-(4′,7′-di-2-thienyl-5′,6′-bis(hexyloxy)-2′,1′,3′-benzothiadiazole)] (PFDTBT-OC6).[52]

3.3 PDI-based polymer acceptors

With regard to the development of PDI-based acceptors, in 2007, Zhan *et al.* first used a PDI-based copolymer, PDI-dithienothiophene copolymer P(PDI-DTT), as a polymer acceptor.[32] The P(PDI-DTT) thin films exhibited a deep LUMO energy of 3.9 eV, a μ_e of 1.3×10^{-2} cm^2 V^{-1} s^{-1} in the field-effect transistor (FET) configuration, and significant absorption ranging from the visible to the near-IR region. A PCE of more than 1% was reported for a device made by blending P(PDI-DTT) with a polythiophene derivative as the donor. Following modulation of the chemical structure of the corresponding donor and acceptor polymers, Zhan *et al.* improved the PCE to 1.48%.[34]

In 2011, a comprehensive study on PDI-based polymer acceptors was conducted by Hashimoto *et al.*[42] These authors synthesized six kinds of PDI-based co-polymers (X-PDI) including those with the co-monomers vinylene (V), thiophene (T), dithienopyrrole (DTP), fluorene (F), dibenzosilole (DBS), and carbazole (C) as X. The highest PCE of 2.23% was achieved for polymer/polymer blend solar cells based on a P3HT analogue incorporating tris(thienylenevinylene) side chains (PT1) and a PDI-carbazole copolymer (PC-PDI). Subsequently, in 2013, Pei *et al.* reported polymer/polymer blend solar cells with a PCE of 2.17%, which were obtained by employing the PDI-dithiophene copolymer (PDI-diTh) as the acceptor and P3HT as the donor.[48] In 2014, Zhan *et al.* utilized binary additives to optimize the blend morphology and achieved a PCE of 3.45% for blend solar cells based on P(PDI-DTT) and PBDTTT-C-T as the acceptor and donor, respectively.[56] Finally, Bao *et al.* reported a PCE of 4.4% for polymer/polymer blend solar cells based on an isoindigo-based polymer donor with polystyrene side chains (PiI-2T-PS5) and a PDI-thiophene copolymer [P(TP)].[57]

3.4 NDI-based polymer acceptors

The first study on the development of an NDI-based copolymer appeared in 2009, when Facchetti *et al.* reported poly[[*N*,*N*′-bis(2-octyldodecyl)-naphthalene-1,4,5,8-bis(dicarboximide)-2,6-diyl]-*alt*-5,5′-(2,2′-bithiophene)] [P(NDI2OD-T2); Polyera ActivInk™ N2200] having a deep LUMO energy of 3.9 eV and remarkable stability under ambient conditions.[78] This polymer exhibited an excellent μ_e of up to 0.45–0.85 cm^2 V^{-1} s^{-1} in the FET configuration and a high μ_e of $>10^{-3}$ cm^2 V^{-1} s^{-1} evaluated from the space-charge limited current.

In the early development stage of these materials, the photovoltaic properties of solar cells utilizing P(NDI2OD-T2) as an acceptor were investigated by blending with donor P3HT. In 2011, the initial P3HT/P(NDI2OD-T2) blend solar cell PCEs were reported to be only 0.21% and 0.17%, by Sirringhaus *et al.*[79] and Fréchet *et al.*,[40] respectively. In the same year, Loi *et al.* obtained a high FF of 0.67 for P3HT/P(NDI2OD-T2) blend solar cells for the first time, which is comparable to the values reported for efficient polymer/fullerene blends.[39] However, the PCE of these devices was 0.16%, because of their limited J_{SC} value of 0.48 mA cm^{-2}. The formation of large domains in the blends, which is driven by preferential segregation and crystallization, is the dominating factor behind the relatively poor J_{SC}, which limits the overall device performance.[80] In 2012, it was found that the addition of chloronaphthalene (CN) suppressed the pre-aggregation of P(NDI2OD-T2) in solution and resulted in a marked improvement in the J_{SC}.[44,81] A PCE of 1.4% with a J_{SC} of 3.77 mA cm^{-2} and a FF of 0.65 was achieved for P3HT/P(NDI2OD-T2) blends prepared from a *p*-xylene and cyanonaphthalene binary mixture as a spin-coating solvent.[44] However, the J_{SC} and PCE values remained significantly lower than those of its P3HT/PCBM counterpart blends, confirming that the morphological characteristics differ between polymer and small molecule acceptor blends.

3.5 Beyond 4%—combination of a low-bandgap polymer donor and rylene diimide-based polymer acceptors

In 2012, McNeill *et al.* combined P(NDI2OD-T2) with a low-bandgap polymer, poly[[4,8-bis[(2-ethylhexyl)oxy]benzo[1,2-b:4,5-b']dithiophene-2,6-diyl][3-fluoro-2-[(2-ethylhexyl)carbonyl] thieno[3,4-b]thiophenediyl]] (PTB7) instead of P3HT.[47] The use of PTB7 as the donor polymer resulted in a spectral response with improved matching to the solar spectrum. An initial PCE of 1.1% was reported, with a peak external quantum efficiency (EQE) of 18% at a wavelength of 680 nm. Marks *et al.* examined the effect of a spin-coating solvent on the device performance of PTB7/P(NDI2OD-T2) blends and improved the PCE up to 2.66% *via* spin-coating from a xylene solution.[55] In 2013, Jenekhe *et al.* reported a PCE of 3.26% for polymer blend solar cells based on poly[(4,4′-bis(2-ethylhexyl)dithieno[3,2-*b*:2′,3′-*d*]silole)-2,6-diyl-*alt*-(2,5-bis(3-(2-ethylhexyl)thiophen-2-yl)thiazolo[5,4-*d*]thiazole)] (PSEHTT) and an NDI-selenophene copolymer (PNDIS-HD).[49] The PSEHTT/PNDIS-HD blend film exhibited balanced electron and hole transport, which explains the high photovoltaic performance. Later, these researchers improved the device performance *via* spin-coating of blend films from a solvent mixture of chlorobenzene and dichlorobenzene, achieving a PCE of 4.8%.[59]

In 2013, Ito *et al.* reported a PCE of 4.1% for polymer/polymer blend solar cells based on poly[2,3-bis-(3-octyloxyphenyl) quinoxaline-5,8-diyl-*alt*-thiophene-2,5-diyl] (PTQ1) and P(NDI2OD-T2).[51] These devices exhibited the highest performance at a PTQ1 fraction of 70 wt%. Also in 2013, Tajima *et al.* reported a PCE of 3.68% for polymer/polymer blend solar cells based on a PTB7 analogue incorporating tris(thienylenevinylene) side chains (TTV7) and an NDI-carbazole copolymer (PC-NDI) as the donor and acceptor, respectively.[50] Owing to the tris(thienylenevinylene) side chains, TTV7 exhibited superior miscibility

with PC-NDI than with PTB7, resulting in a well-mixed blend morphology and, hence, an improved photocurrent. In 2014, Ito *et al.* reported a PCE of 5.7% for polymer/polymer blend solar cells based on poly[[2,6'-4,8-di(5-ethylhexylthienyl)benzo[1,2-*b*;3,3-*b*]dithiophene][3-fluoro-2[(2-ethylhexyl)carbonyl]thieno-[3,4-*b*]thiophenediyl]] (PTB7-Th) and P(NDI2OD-T2).[61] The main reason for this high PCE was that both the generation and collection efficiencies of the free charge carriers were as high as 80%; these values are comparable to those for polymer/fullerene blend solar cells, which suggests that there is no inherent disadvantage to polymer/polymer blend solar cells.

In 2015, Kim *et al.* reported polymer/polymer blend solar cells based on poly[(2,5-bis(2-hexyldecyloxy)phenylene)-*alt*-(5,6-difluoro-4,7-di(thiophen-2-yl)benzo[*c*][1,2,5]thiadiazole)] (PPDT2FBT) and P(NDI2OD-T2).[71] The device PCE increased from 1.54% to 3.59% with the increase in the PPDT2FBT M_n from 12 000 to 40 000 g mol^{-1}. The PCE was further improved to 5.10% when diphenylether (DPE) was used as an additive. In 2015, Kim *et al.* reported polymer/polymer blend solar cells based on PTB7-Th and a series of NDI-thiophene copolymers (PNDIT-R, R = alkyl) with different side chains.[73] The phase-separated domain size in the blend exhibited a sensitive dependence on the side chains, and was suppressed to the greatest extent for PNDIT-HD with a 2-hexyldecyl group. As a result, the highest PCE of 5.96% was obtained for PTB7-Th/PNDIT-HD blend solar cells. Kim *et al.* further reported polymer/polymer blend solar cells based on poly[4,8-bis(5-(2-ethylhexyl)thiophen-2-yl)benzo[1,2-*b*:4,5-*b*']dithiophene-*alt*-1,3-bis-(thiophen-2-yl)-5-(2-hexyldecyl)-4*H*-thieno[3,4-*c*]pyrrole-4,6(5*H*)-dione] (PBDTTTPD) as a donor and poly[[*N*,*N*'-bis(2-hexyldecyl)-naphthalene-1,4,5,8-bis(dicarboximide)-2,6-diyl]-*alt*-5,5'-thiophene] (PNDIT-HD) as an acceptor. The PBDTTTPD/PNDIT-HD blend solar cells exhibited a PCE of 6.64% with a relatively large V_{OC} of 1.06, due to the deep HOMO energy level of the donor PBDTTTPD (−5.49 eV).[14] In the same year, Jen *et al.* synthesized P(NDI2OD-T2) derivatives containing a fluorinated dithiophene unit in the main chain, P(NDI2DT-FT2). Fluorination on the polymer backbone leads to enhanced crystallinity and electron transport ability, and also enlarges the HOMO–LUMO band gap of the polymer acceptor. Consequently, the PTB7-Th/P(NDIDT-FT2) blend solar cells exhibited higher FF and larger V_{OC} values than those of the corresponding PTB7-Th/P(NDI2OD-T2) blends, yielding a higher PCE of 6.71%.[75] Also in 2015, Jenekhe *et al.* reported polymer/polymer blend solar cells based on a benzodithiophene-thieno[3,4-*b*]thiophene copolymer (PBDTTT-C-T) and a series of NDI-selenophene/PDI-selenophene random copolymers (*x*PDI, *x* = 10, 30, or 50 mol%).[74] The PBDTTT-C-T/30PDI blend films exhibited the optimal phase-separated morphology and, hence, yielded the highest PCE of 6.29%. Notably, the maximum value of the external quantum efficiency (EQE) exceeded 90%, and the J_{SC} was as high as 18.55 mA cm^{-2}.

Very recently, Jenekhe *et al.* reported a remarkable improvement in the photocurrent of polymer blend solar cells based on PTB7-Th and an NDI-selenophene copolymer (PNDIS-HD), obtained *via* a simple film aging process.[76] The optimum PCE of 7.73% with a J_{SC} of 18.8 mA cm^{-2} and a maximum EQE of 85% was obtained after the film was aged in a glovebox at room temperature for 72 h; this value is significantly larger than the PCE of 3.66% that was obtained following thermal annealing at 175 °C for 10 min. It is worth noting that the highest yet achieved PCE of 8.27% was reported by Li *et al.* during the preparation of this review.[77] This high PCE was achieved for a polymer/polymer blend based on a medium-bandgap benzodithiophene-*alt*-benzotriazole copolymer (J51) and low-bandgap P(NDI2OD-T2) pair, as the donor and acceptor, respectively. A large J_{SC} of 14.18 mA cm^{-2} due to complementary absorption from visible to near-IR wavelengths, along with an excellent FF approaching 0.7, are key components in order to obtain a PCE of more than 8%.

Certified polymer/polymer blend solar cells with a PCE of 6.47% have been demonstrated by the Polyera Corporation team, although the materials have not been disclosed. This PCE was certified by the National Renewable Energy Laboratory, and this is the highest certified performance of a polymer/polymer blend solar cell to date.[82]

4. Blend morphology control

Simple spin-coating of the photoactive layer from a blend solution of polymers in a single solvent usually results in an undesirable morphology, with problematic features such as large phase separation,[83] inhomogeneous internal phase composition,[80,84–86] and reduced ordering of the polymer chains;[87] this morphology is known to correlate with poor device performance. Therefore, control of the morphology of polymer/polymer blends is an important aspect of the recent remarkable enhancement of the resultant PCEs, in conjunction with the synthesis of new polymer acceptors. Optimization of the blend morphology has been attempted using processing techniques such as solvent engineering (using low-boiling-point (low-bp) solvents, mixed solvents, solvent additives) and thermal annealing, or by adjusting the polymer molecular weight, donor/acceptor blending ratios, and chemical structures of the polymer side chains. These techniques can affect the degree of phase separation, the polymer chain ordering, and the orientation of the crystalline domains in the blend films, thereby facilitating the formation of a morphology preferable to charge generation and transport. Among these processing methods, studies on solvent engineering, thermal annealing, polymer molecular weight, donor/acceptor (D : A) blend ratios, and the use of polymer nanowires are reviewed here. Further, we discuss the recent research progress with regard to the preparation and application of fully conjugated donor–acceptor block copolymers as the photoactive layers of polymer solar cells.

4.1 Solvent engineering

4.1.1 Solvent boiling points. When insufficient time is allowed for complete phase separation of the polymer blend, an intermediate state of mixing is frozen into the solid state. Therefore, controlling the film formation kinetics is one approach to obtaining the desired phase-separated

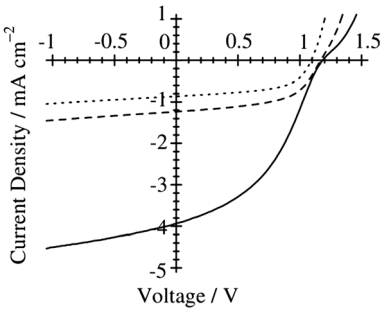

Fig. 9 *J–V* characteristics of P3HT/PF12TBT solar cells under AM 1.5G 100 mW cm^{-2} illumination. The devices were fabricated *via* spin-coating from DCB (dotted line), CB (dashed line), and CF (solid line) solutions of P3HT and PF12TBT (1 : 1 weight ratio) and annealed at 140 °C for 10 min. Adapted with permission from (ref. 41). Copyright 2011, American Chemical Society.

morphology, which allows optimization of the photovoltaic performance. Experimentally, the polymer blend morphology is varied by the selection of different spin-coating solvents. Rapid quenching of the kinetics, which occurs in processing from a low-bp solvent, produces films in a single phase or an intermixed region of the phase diagram, resulting in well-mixed structures.

Ito *et al.* have studied the effect of the choice of the spin-coating solvent on the device performance of polymer/polymer blend solar cells based on a semicrystalline donor P3HT and an amorphous acceptor PF12TBT.[41] Fig. 9 shows the current density–voltage (*J–V*) characteristics of P3HT/PF12TBT blend solar cells fabricated from spin-coating solutions with different bp solvents: *o*-dichlorobenzene (DCB, bp = 181 °C), chlorobenzene (CB, bp = 132 °C), and chloroform (CF, bp = 61 °C). The J_{SC} was as low as 1 mA cm^{-2} for the devices fabricated from the high-bp solvents (DCB and CB). In contrast, a significant increase in J_{SC} to 4 mA cm^{-2} was observed for the device fabricated from the low-bp solvent (CF).

In addition, atomic force microscopy (AFM) revealed marked differences in the surface morphologies of the three blend films (Fig. 10). For the blend film spin-coated from DCB, phase-separated structures were clearly observed: each domain had a lateral dimension of a few micrometers. For the blend film fabricated from CB, smaller but still distinct phase-separated structures were observed: each domain had a lateral dimension of a few hundred nanometers. In either case, the phase-separated domains were significantly larger than the L_D value of typical conjugated polymers (≤10 nm).[19] In contrast, no distinct phase-separated structure was observed for the blend film fabricated from CF, suggesting a well-mixed blend morphology of P3HT and PF12TBT comparable to L_D. Suppressing the spontaneous growth of phase separation during spin-coating is the key to obtaining devices with large J_{SC} based on polymer/polymer blend systems.

4.1.2 Solvent additives and film aging. Processing approaches using solvent additives are known to be useful for inducing optimal blend nanostructures correlated with high PCEs for polymer/fullerene blend solar cells.[88] The positive effects of solvent additives on the device performance have also been reported for polymer/polymer blend systems. In 2012, Friend *et al.* examined the effect of additives on the efficiency of polymer/polymer blend solar cells based on a P3HT donor and a range of acceptors, systematically and for the first time.[89] They demonstrated that 4-bromoanisole (BrAni) is an effective solvent additive for the promotion of P3HT crystallization and increased hole mobility (μ_h) in P3HT-containing blends. The addition of BrAni (2–14 vol%) increased the EQE to more than 10% for both P3HT/F8TBT and P3HT/poly[*N*-9′-heptadecanyl-2,7-carbazole-*alt*-5,5-(4′,7′-di-2-thienyl-2′,1′,3′-benzothiadiazole)] (PCDTBT) blend solar cells prepared from CB solution. These researchers further revealed that a combination of a solvent additive and post-thermal annealing yields a greater improvement in the EQE and J_{SC} than additive processing alone. Further, Neher *et al.* demonstrated for the first time that the addition of CN to a *p*-xylene solution suppresses the pre-aggregation of P(NDI2OD-T2) in the solution.[44,81] P3HT/P(NDI2OD-T2) blend solar cells prepared from a *p*-xylene : CN (50 : 50) mixed solvent exhibited a large increase in J_{SC} and PCE due to the finer mixing of polymers in the film, compared with reference devices obtained from pure *p*-xylene (Fig. 11).

Recent studies by Kim *et al.* have shown that additives enhance the order of P(NDI2OD-T2) chains in blend films and improve the device PCE.[58,71] For PTB7-Th/P(NDI2OD-T2) blend solar cells prepared from a CF solution, the addition of 1,8-diiodooctane (DIO) (1.25 vol%) enhances the crystallinity of P(NDI2OD-T2) and causes an increase in μ_e by a factor of more than 10, while maintaining proper mixing of the polymers. Consequently, J_{SC} increases in the presence of DIO, boosting the PCE to 4.60% from 3.41%.[58] A similar positive effect of an

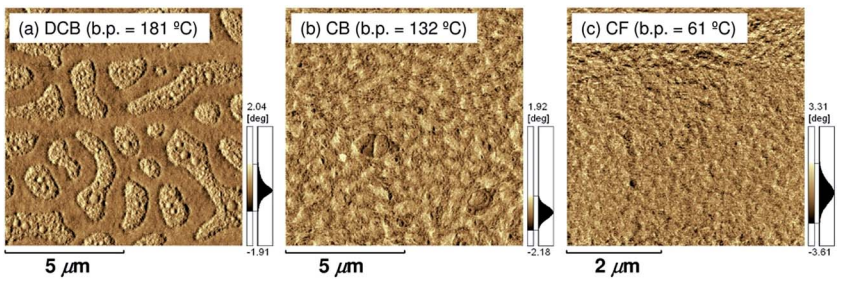

Fig. 10 AFM phase images of P3HT/PF12TBT blend films spin-coated from (a) DCB (b) CB, and (c) CF solutions of P3HT and PF12TBT (1 : 1 weight ratio), on glass substrates and annealed at 140 °C for 10 min.

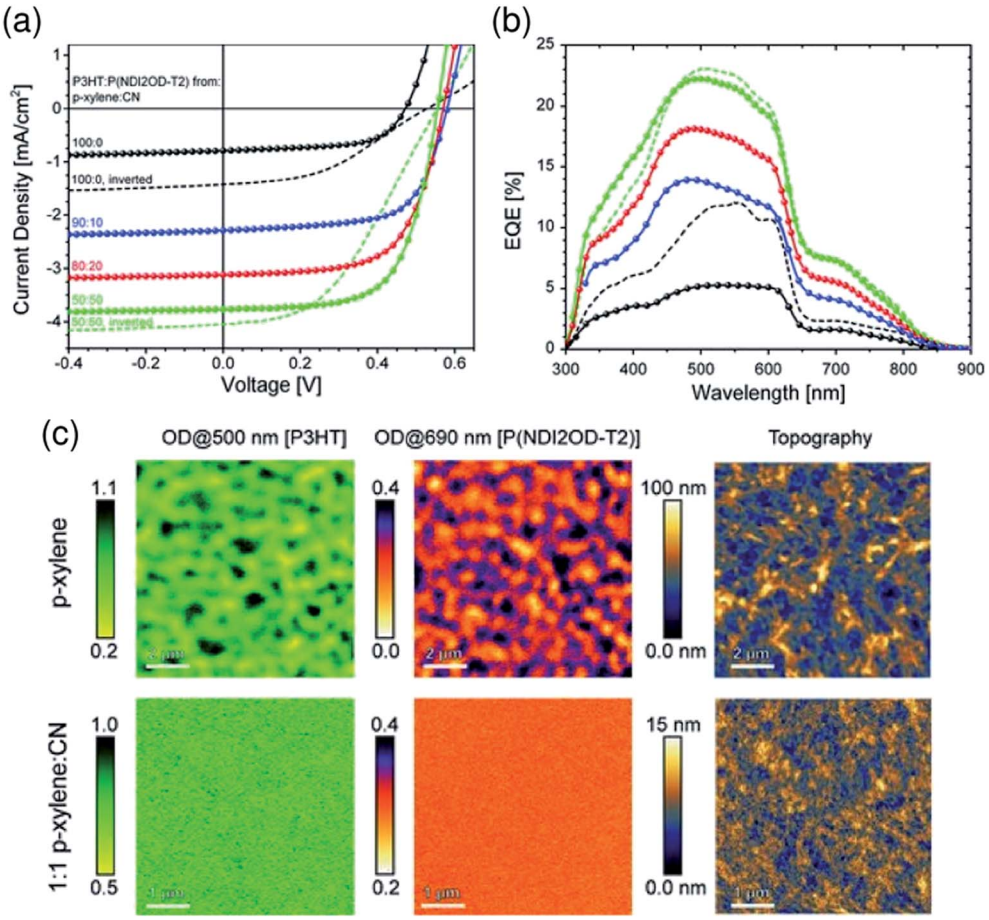

Fig. 11 (a) *J*–*V* characteristics and (b) corresponding EQE spectra of P3HT/P(NDI2OD-T2) BHJ solar cells under simulated AM 1.5 illumination. The blend layer was spin-coated from solvent mixtures of *p*-xylene and CN. The *p*-xylene : CN mixing ratios are 100 : 0 (black), 90 : 10 (blue), 80 : 20 (red), and 50 : 50 (green). (c) Near-field scanning optical microscopy (SNOM) images of blends of corresponding solar cells fabricated from *p*-xylene (top) and 1 : 1 *p*-xylene : CN (bottom), taken at 500 and 690 nm in order to probe the P3HT and P(NDI2OD-T2) fractions of the blend, respectively. The scale bar is expressed in terms of the optical density (OD), defined *via* $OD = -\log_{10}(I/I_0)$, where I_0 and I are the incident and transmitted photon fluxes, respectively. The AFM height images were obtained from independent measurements using a Si-cantilever. Reproduced with permission from (ref. 44). Copyright 2012, Wiley-VCH Verlag GmbH & Co. KGaA, Weinheim.

additive on the P(NDI2OD-T2) crystallinity and μ_e has also been observed for PPDT2FBT/P(NDI2OD-T2) blend solar cells prepared from a CF solution. The addition of DPE (1.0 vol%) was found to primarily increase J_{SC}, which boosted the PCE to 5.10% from 3.59%.[71] Hou *et al.* have reported that the FF is enhanced from 0.530 to 0.596 through the use of CN (3 vol%) as an additive for PBDTBDD-T/PBDTNDI-T blend solar cells prepared from CB.[66] These researchers ascribed the improvement in the FF to the higher domain purity and enhanced molecular ordering of the blend film, as induced by processing with CN. Consequently, the device PCE was improved from 2.18% to 2.88%. In addition, Zhan *et al.* have demonstrated that binary additives synergistically boost the efficiency of a polymer/polymer blend solar cell.[56] These researchers used PDI-2DTT and DIO as additives for PBDTTT-C-T/P(PDI-DTT) blend solar cells prepared from DCB (Fig. 12). In this configuration, the additive PDI-2DTT suppresses aggregation of the P(PDI-DTT) acceptor and enhances the donor/acceptor mixing, while the DIO facilitates aggregation and crystallization of the donor PBDTTT-C-T. Consequently, the combination of PDI-2DTT (2 wt%) and DIO (6 vol%) leads to suitable phase separation and improved and balanced charge carrier mobilities, which enhance both J_{SC} and FF and boost the PCE to 3.45% from 1.18%.

Very recently, Jenekhe *et al.* applied film aging to control the blend morphology of polymer/polymer blend solar cells.[76] In that study, blend films comprised of a PTB7-Th donor with a PNDIS-HD acceptor were prepared *via* spin-coating from a CB solution, and the wet films were placed in an argon-filled glovebox to dry at room temperature for 72 h. The slow self-organization of the blends facilitated by the slow solvent evaporation at room temperature resulted in enhanced μ_e, smaller mean crystalline domain sizes, and the existence of a more amorphous mixed region compared to the control blend films, which were processed using thermal annealing after spin-coating. The resultant PTB7-Th/PNDIS-HD blend solar cells exhibited a PCE of 7.7% and a J_{SC} of 18.8 mA cm^{-2}, with a maximum EQE of 85% (Fig. 13).

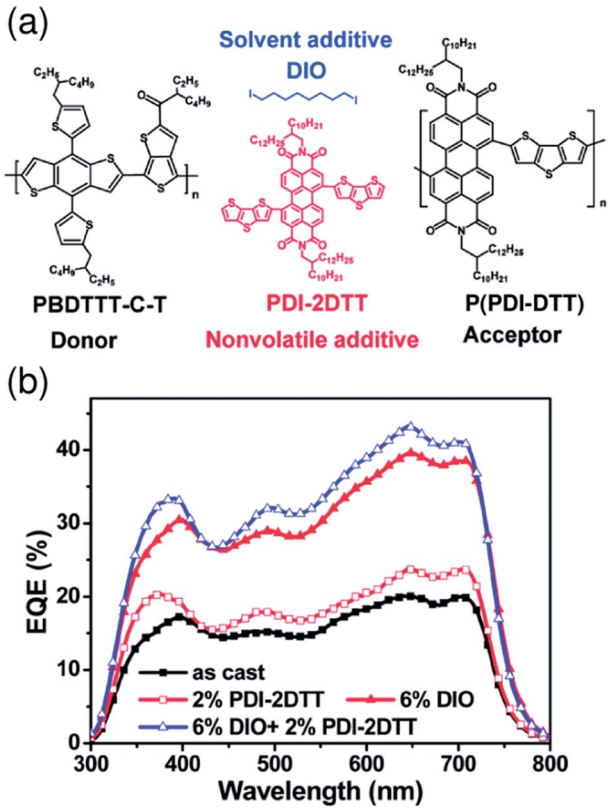

Fig. 12 (a) Chemical structures of the PBDTTT-C-T donor, P(PDI-DTT) acceptor, PDI-2DTT, and DIO. (b) EQE spectra of PBDTTT-C-T/P(PDI-DTT) blend solar cells without or with additives under AM 1.5G solar simulator illumination at 100 mW cm^{-2}. Reproduced with permission from (ref. 56). Copyright 2013, The Royal Society of Chemistry.

4.2 Thermal annealing

Thermal annealing of finely mixed blend films provides a convenient means for tuning the domain size from a few nanometers to tens of nanometers. Previously, Ito *et al.* have investigated the effect of nanoscale phase separation on device performance.[41,90] Fig. 14a shows the observed annealing temperature dependence of the photovoltaic parameters of a P3HT/PF12TBT blend solar cell fabricated *via* spin-coating from a CF solution.[41] The as-spun device exhibited a very small J_{SC} and FF before annealing, and the PCE was as low as 0.27%. However, the device performance after annealing for 10 min had a significant dependence on the annealing temperature, and the highest PCE of 2.0% was obtained following annealing at 140 °C.

Note that the PL of a constituent polymer is quenched when polymer excitons generated in the blend film can arrive at the interface with other polymers. Therefore, the PL quenching efficiency (Φ_q) provides information about the size and purity of the domains on a length scale comparable to L_D. In Fig. 14b, J_{SC} is plotted against the Φ_q values of PF12TBT, in order to extract the relationship between the blend nanomorphology and J_{SC}. The high value of the Φ_q (~90%) of the as-spun film indicates a well-mixed blend structure with a domain size close to L_D. Further, the measured Φ_q values remained as high as 80–90%, even for films annealed at 80–120 °C. On the other hand, J_{SC} increased steeply from 1.1 mA cm^{-2} for the as-spun device to 4.2 mA cm^{-2} for the device annealed at 120 °C. In contrast, both Φ_q and J_{SC} decreased following annealing at temperatures above 120 °C.

This behavior suggests that thermal annealing causes two-step structural changes in the blend. In the first step, for temperatures up to 120 °C, the small but phase-separated domains are purified by expulsion of the minor component polymer chains. The PF12TBT-rich domains in the as-spun blend film seem to involve minor P3HT chains. The isolated P3HT chains in the PF12TBT matrix can serve as charge transfer/quenching sites for PF12TBT excitons, but cannot contribute to the photocurrent, because the resultant holes on the P3HT chains have no pathways to the electrode. The annealing treatment below 120 °C induces homogeneity between the individual domains in the compositions, while keeping the domain size close to L_D. In that case, J_{SC} increases with annealing at elevated temperature. In the second step, thermal annealing at temperatures higher than 120 °C causes enlargement of the phase-separated structures, which is accompanied by growth of the domain size beyond L_D and a decrease in the domain interface area. These structural changes reduce both Φ_q and J_{SC}.

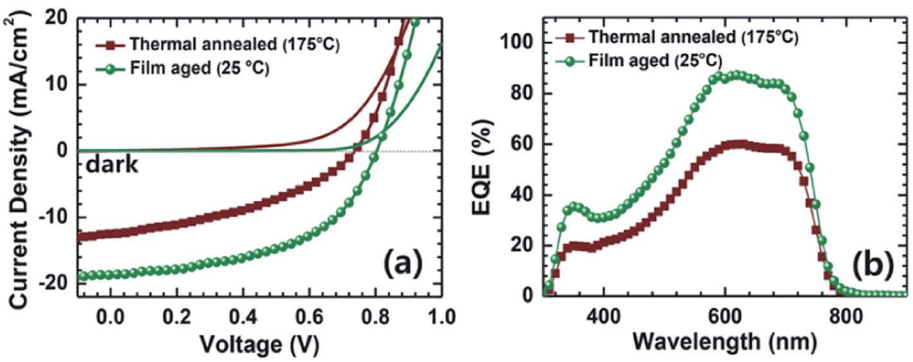

Fig. 13 (a) *J*–*V* curves and (b) EQE spectra of PTB7-Th/PNDIS-HD (1 : 1 w/w) blend solar cells with thermally annealed (175 °C, 10 min) or film-aged (25 °C, 72 h) active layers. Adapted with permission from (ref. 76). Copyright 2015, Wiley-VCH Verlag GmbH & Co. KGaA, Weinheim.

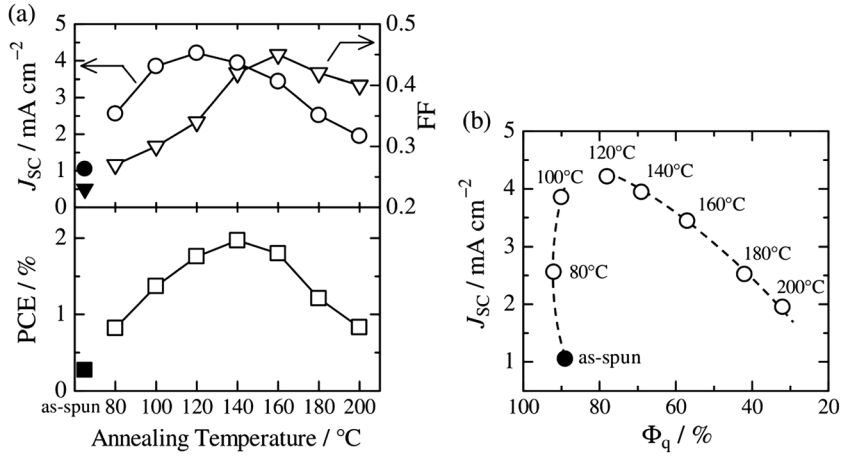

Fig. 14 (a) Device parameter dependence on annealing temperature: J_{SC} (open circles), FF (open inverted triangles), and PCE (open squares). The solid symbols represent the device parameters before thermal annealing. (b) Plots of J_{SC} against the respective Φ_q value of PF12TBT. These parameters were measured for P3HT/PF12TBT blend solar cells fabricated *via* spin-coating from a CF solution of P3HT and PF12TBT (1 : 1 weight ratio). The broken lines are guides for the eye. Reproduced with permission from (ref. 41). Copyright 2011, American Chemical Society.

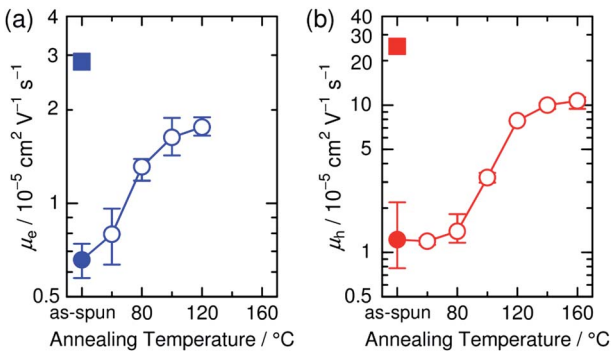

Fig. 15 (a) Electron and (b) hole mobilities of P3HT/PF12TBT blend films (circles) with respect to annealing temperature. The squares in (a) and (b) indicate the electron and hole mobilities, respectively, of the as-spun PF12TBT neat and as-spun P3HT neat films. Reproduced with permission from (ref. 91). Copyright 2015, Wiley-VCH Verlag GmbH & Co. KGaA, Weinheim.

The increase in the FF with thermal annealing can be explained in terms of the improved charge carrier mobility, as shown in Fig. 15.[91] The value of μ_e increases steadily with temperature even in the temperature range below 120 °C, suggesting that the PF12TBT-rich amorphous domains increase in purity, even if the domain coarsening is frozen. The electron transport is improved by the exclusion of the isolated P3HT chains from the PF12TBT domains. Meanwhile, thermal annealing increases the value of μ_h, because it promotes ordering of the semicrystalline P3HT chains and growth of the adjacent P3HT nanodomains, resulting in the formation of an electrically interconnected crystalline phase for hole transport. Because of the annealing temperature dependence of J_{SC} and FF, the maximum PCE is obtained through annealing at 140 °C, which establishes a balance between charge generation and transport. Ito *et al.* have also spectroscopically investigated morphology-dependent charge generation and recombination properties in P3HT/PF12TBT blends using transient absorption (TA) measurements, which were then correlated with the temperature dependence of the device EQEs.[91]

4.3 Polymer molecular weight

Ito *et al.* have studied the influence of the M_w on the device performance of blends based on P3HT and PF12TBT, using three PF12TBTs with different M_w's: L-PF12TBT ($M_w = 8500$), M-PF12TBT ($M_w = 20\,000$), and H-PF12TBT ($M_w = 78\,000$).[46] The photovoltaic performance exhibited the following dependence on M_w:

- The PCE improved from 1.9 to 2.7% with increasing M_w;
- The optimal annealing temperature that yields the maximum PCE increased from 100 to 120 and then to 140 °C with increasing M_w;
- The improvement in the PCE can primarily be ascribed to an increase in the FF, as both J_{SC} and V_{OC} are almost identical among the three optimized devices.

Fig. 16 shows the *J*–*V* characteristics of P3HT/L-PF12TBT and P3HT/H-PF12TBT solar cells. Following thermal annealing at 100 °C (broken lines), which yielded the optimum PCE for P3HT/L-PF12TBT, J_{SC} reached a maximum value of 4 mA cm^{-2} for both P3HT/L-PF12TBT and P3HT/H-PF12TBT. On the other hand, the FF was still as low as 0.41 for P3HT/L-PF12TBT and 0.37 for P3HT/H-PF12TBT. Following annealing at an elevated temperature of 140 °C (solid lines), the FF increased and reached 0.50 for P3HT/L-PF12TBT and 0.55 for P3HT/H-PF12TBT. However, such high-temperature annealing yielded a significantly decreased J_{SC} for P3HT/L-PF12TBT. On the other hand, it was possible to maintain the maximum value of J_{SC} for P3HT/H-PF12TBT. Consequently, the PCE of P3HT/H-PF12TBT could be improved even after annealing at 140 °C, and this specimen yielded the highest PCE value of 2.7% among the examined devices. As shown in Fig. 16, high-temperature annealing is required in order to improve the PCE, because of

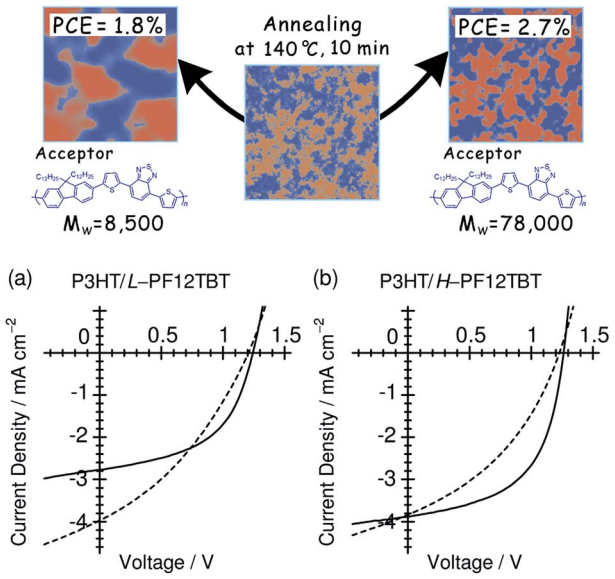

Fig. 16 *J–V* characteristics of (a) P3HT/L-PF12TBT and (b) P3HT/H-PF12TBT blend solar cells under AM 1.5G illumination from a calibrated solar simulator with an intensity of 100 mW cm^{-2}. The device was fabricated by spin-coating a CF solution of P3HT and PF12TBT (1 : 1 weight ratio) and annealed at 100 °C (broken lines) and 140 °C (solid lines) for 10 min. Reproduced with permission from (ref. 46). Copyright 2012, American Chemical Society.

its positive effect on the FF. On the other hand, small domain structures comparable in size to L_D should be retained during annealing. Ito *et al.*'s study[46] demonstrates that the ideal blend morphology that yields both large J_{SC} and FF values at the same time is achieved using H-PF12TBT. In a device with high-M_w PF12TBT, efficient charge generation is maintained even at high annealing temperatures, because the rate of domain bloating decelerates owing to the reduced diffusion mobility of the PF12TBT chains. On the other hand, the charge collection efficiency also increases during the annealing, through both domain purification of the PF12TBT and ordering of the P3HT chains.

Kim *et al.* have studied the effect of the polymer molecular weight on the photovoltaic characteristics of blends based on a pair of semicrystalline donor PPDT2FBT and P(NDI2OD-T2) acceptor polymers, PPDT2FBT/P(NDI2OD-T2), using three PPDT2FBTs with different M_n's: PPDT2FBT$_L$ (M_n = 12 000), PPDT2FBT$_M$ (M_n = 24 000), and PPDT2FBT$_H$ (M_n = 40 000).[71] These researchers fabricated the devices *via* spin-coating from a CF solution and compared their performances (Fig. 17).

The photovoltaic performance was found to exhibit the following dependence on M_n:

- The PCE was improved from 1.54 to 3.59% with increasing M_n;
- The improvement in the PCE was primarily ascribed to an increase in the J_{SC}, as both FF and V_{OC} were almost identical among the three devices;
- The DPE additive improved the J_{SC} and FF and, thus, the PCE values for all PPDT2FBT/P(NDI2OD-T2) blends in a similar manner, independent of their M_n.

The crystalline ordering and blend morphologies of the blends with different M_n were examined using grazing incident X-ray scattering, resonant soft X-ray scattering, and AFM measurements. The results suggest that high-M_n PPDT2FBT$_H$ promotes a preferential face-on crystalline orientation of PPDT2FBT in the blend film, and facilitates intermixing between PPDT2FBT and P(NDI2OD-T2) with a smaller domain size. The PPDT2FBT$_H$/P(NDI2OD-T2) blend morphology contributes to an improvement in both the charge generation efficiency and charge transport, thereby increasing the J_{SC} and PCE values. The incorporation of DPE induces an increase in the μ_e values for all PPDT2FBT/P(NDI2OD-T2) blends. As a result, the μ_e becomes more balanced with the μ_h, further improving the J_{SC}, FF, and PCE values.

4.4 Donor/acceptor blend ratio

The D : A blend ratio is an important parameter with regard to the fabrication of polymer/polymer blend solar cells. Ito *et al.* have investigated the effect of the D : A ratio on the photovoltaic performance of polymer/polymer blend solar cells based on an amorphous donor PTQ1 and a semicrystalline acceptor P(NDI2OD-T2).[51] Fig. 18 shows the photovoltaic performance of PTQ1/P(NDI2OD-T2) blend solar cells with various D : A ratios. The photovoltaic parameters depend strongly on the D : A ratio. In particular, both J_{SC} and FF increase remarkably with increases in the PTQ1 content, and the highest PCE of 4.1% is

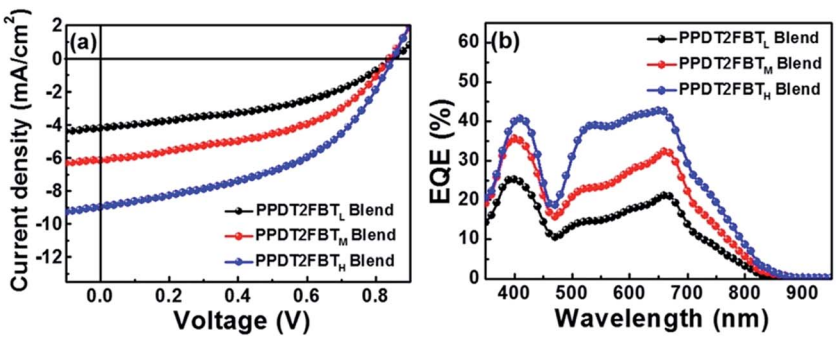

Fig. 17 (a) *J–V* characteristics and (b) EQE spectra of PPDT2FBT/P(NDI2OD-T2) blend solar cells. Adapted with permission from (ref. 71). Copyright 2015, American Chemical Society.

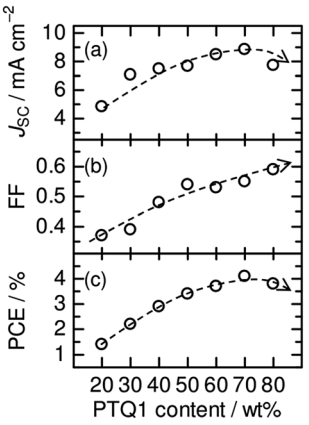

Fig. 18 Photovoltaic parameters (J_{SC}, FF, PCE) of PTQ1/N2200 blend solar cells with various D : A ratios. The broken lines are guides for the eye. Reproduced with permission from (ref. 51). Copyright 2013, Wiley-VCH Verlag GmbH & Co. KGaA, Weinheim.

realized for the device with D : A = 70 : 30. This marked PCE dependence demonstrates the importance of controlling the D : A blend ratio for the improvement of the overall device performance. In their study, Ito *et al.* investigated the charge generation and transport efficiency of blended films with different D : A ratios.

Fig. 19a shows the Φ_q values of P(NDI2OD-T2) and PTQ1 for blend films, which represent the efficiency of charge generation from P(NDI2OD-T2) and PTQ1 excitons, respectively. The Φ_q value of P(NDI2OD-T2) decreased markedly with increasing P(NDI2OD-T2) content. On the other hand, that of PTQ1 was greater than 96% for all of the blend films, regardless of the D : A ratio. Consequently, the overall charge generation efficiency in the blend film increased with increasing PTQ1 content, which is key to obtaining large J_{SC}. In the corresponding report, Ito *et al.* considered the long-range resonant (Förster-type) energy transfer in order to explain the large Φ_q value of PTQ1 for all D : A compositions.[92,93] Fig. 19b shows the dependence of μ_h and μ_e on the D : A ratio. The value of μ_h increased with increasing PTQ1 content. In contrast, μ_e remained significantly higher than μ_h for all the blended compositions. As a result, μ_h became more balanced with the large μ_e as the PTQ1 content increased. This result reveals that control of the D : A ratio is essential to achieving a balance between μ_h and μ_e, which is key to obtaining high FFs.

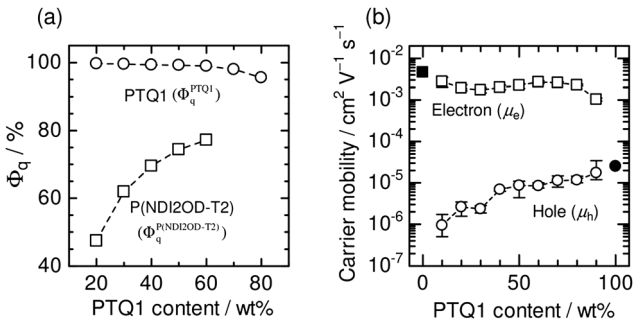

Fig. 19 (a) PL quenching efficiencies (Φ_q) of PTQ1 (circles) and P(NDI2OD-T2) (squares) in PTQ1/P(NDI2OD-T2) blend films as functions of PTQ1 weight percentage. (b) Hole (open circles) and electron (open squares) mobilities in PTQ1/N2200 blend films as functions of PTQ1 weight percentage. The solid circle and square indicate the hole and electron mobilities in the PTQ1 and P(NDI2OD-T2) neat films, respectively. Reproduced with permission from (ref. 51). Copyright 2013, Wiley-VCH Verlag GmbH & Co. KGaA, Weinheim.

The D : A ratio that yields the optimal FF differs between the PTQ1/P(NDI2OD-T2) and conventional polymer/PCBM blend solar cells. For polymer/PCBM blends, the PCBM concentration should be sufficiently high to ensure the presence of sufficient electron transport networks throughout the film. For example, in blends with amorphous donor polymers, such as MDMO-PPV,[94] fluorene copolymers,[95] and PCDTBT,[96] 80 wt% PCBM is required in order to provide an optimal FF. In contrast, as an acceptor, P(NDI2OD-T2) can provide sufficient pathways for electron transport through the chain networks, even when the concentration is as low as 10 wt% (see Fig. 19b). The preferable formation of interpenetrating networks by both the polymer donor and acceptor allows for adjustment of the D : A blend ratio in a wide range, without loss of charge transport pathways. As shown in Table 1 (see the D : A blend ratio column), the device performance can be maximized with acceptor fractions lower than 33 wt% for other combinations of donor and acceptor polymers,[34,42,45,50,51,62,64,67,70,77] which are typical for devices based on polymer acceptors.

4.5 Use of self-assembled polymer nanowires

Self-assembled nanostructures of semiconducting polymers have been recognized as active building components for photovoltaic applications. Polymer nanowires, which can be grown in solution through the aggregation and crystallization of semiconducting polymer chains in a quasi-one-dimensional fashion, are of particular interest, because of their structural features (widths comparable to L_D and lengths of several micrometers).[97–100] Regioregular poly(3-alkylthiophene) (P3AT) nanowires have been widely examined for blends with fullerenes.[97,98] The potential advantages of applying polymer nanowires in BHJ solar cells are as follows: (1) polymer nanowires offer large donor/acceptor interfacial areas for efficient exciton dissociation, while also providing electrically interconnected pathways for efficient charge transport; (2) the high crystallinity of the nanowires yields high carrier mobilities and high absorption coefficients; (3) it is not necessary to improve the crystallinity of a constituent polymer *via* thermal and solvent annealing, which often causes domain coarsening and decreases the J_{SC}.

Recently, polymer nanowires have been applied as a means of controlling the nanomorphology in polymer/polymer blend solar cells.[53,101] This approach was employed for the first time in 2010, when Lam *et al.* used P3HT nanowires to control the polymer/polymer blend morphology.[101] These researchers prepared P3HT nanowires through gradual cooling of P3HT solution in a marginal *p*-xylene solvent. Subsequently, the P3HT-nanowire suspension was mixed with poly(9,9-dioctylfluorene-*alt*-benzothiadiazole) (F8BT) at a 1 : 1 weight ratio, followed by spin-coating of the solution without filtration. The

P3HT-nanowire/F8BT blend solar cells increased the J_{SC} by a factor of 10 (from 0.029 to 0.291 mA cm^{-2}) compared to an as-cast device based on a P3HT/F8BT blend spin-coated from a DCB solution. Further, in 2014, Li *et al.* applied crystalline P3HT nanowires to a blend with F8TBT.[53] These researchers prepared a P3HT-nanowire suspension in a good DCB solvent by slowly and gradually adding a poor *n*-hexane solvent to the DCB solution with P3HT. Subsequently, F8TBT was added to the P3HT-nanowire suspension to yield a P3HT-nanowire : F8TBT (1 : 1 weight ratio) mixture. The solution was then spin-coated without filtration. Transmission electron microscopy revealed that the P3HT-nanowire/F8TBT blend films contained homogeneously distributed P3HT nanowires with widths of ~20 nm and lengths of ~5 μm (Fig. 20). The P3HT-nanowire/F8TBT blend solar cells exhibited a J_{SC} of 3.29 mA cm^{-2}, an V_{OC} of 1.35 eV, and a FF of 0.42; consequently, a PCE of 1.87% was achieved after thermal annealing. The J_{SC} and FF values of the P3HT-nanowire/F8TBT blend were significantly enhanced compared to those of the as-cast and thermally annealed devices based on a P3HT/F8TBT blend spin-coated from a DCB solution (Fig. 21). These studies demonstrate the potential of polymer nanowire application for both rational control of film morphology and for efficiency enhancement of polymer/polymer blend solar cells.

We further note that the self-assembly nanowire techniques are applicable not only to polymer donors,[102–104] but also to polymer acceptors.[105,106] Polymer solar cells made from blends of polymer nanowires as both donor and acceptor components will enhance the feasibility of designing a nanoscale morphology consisting of a highly crystalline and pure charge-transport network. These all-polymer-nanowire systems could introduce a new avenue for accelerated enhancement of polymer photovoltaic efficiency; however, such systems have not yet been explored or demonstrated.

4.6 Use of fully conjugated donor–acceptor block copolymers

Donor–acceptor diblock copolymers are a fascinating and academically challenging subject with regard to photovoltaic applications, because diblock copolymers self-assemble into well-ordered and thermodynamically stable nanostructures with domain sizes commensurate to L_D through control of the individual block lengths.[107–109] In 2000, Hadziioannou *et al.* reported an attempt to enhance the photovoltaic efficiency of donor–acceptor block polymers.[110]

In the early development stages, the majority of donor–acceptor block copolymers were composed of a conjugated donor polymer and a non-conjugated backbone attached to acceptor units in the side chain. Such copolymers have poor photovoltaic properties, because the non-conjugated backbone is neither optically nor electronically active. To overcome this disadvantage, recently, fully conjugated donor–acceptor block copolymers have been developed for photovoltaic applications (Fig. 22).[111–114] In 2010, Hashimoto *et al.* synthesized P3HT-based diblock copolymers (P3HT-*b*-P3HTPCBM) consisting of a P3HT block and a P3AT block with a fullerene in a part of the side chain.[115] The block copolymer film exhibited microphase separation patterns of ~20 nm in size. These researchers applied the P3HT-*b*-P3HTPCBM to single-component solar cells and obtained a PCE of 1.70% with a J_{SC} of 6.15 mA cm^{-2}, an V_{OC} of 0.54 V, and a FF of 0.51. The relatively high FF suggests that efficient charge transport networks were constructed in the diblock copolymer films.

Subsequently, in 2011, Mulherin *et al.* synthesized a fully conjugated donor–acceptor diblock copolymer poly(3-hexylthiophene)-*block*-poly{[9,9-bis-(2-octyldodecyl)fluorene-2,7-diyl]-*alt*-[4,7-di(thiophene-2-yl)-2,1,3-benzothiadiazole]-5′,5″-diyl} (P3HT-*b*-PFTBTT).[116] By adding P3HT-*b*-PFTBTT to the P3HT/PFTBTT homopolymer blend as a compatibilizer, phase separation of the active layers was restricted to a length scale of 25 nm in the lateral direction, even following thermal annealing above the melting temperature of P3HT. The J_{SC} and PCE of the ternary blend device increased continually with the annealing temperature and remained stable up to 220 °C. However, the J_{SC} of the homopolymer blend device began to decrease at temperatures above 130 °C, because the morphology became too coarse for efficient charge generation.

In 2012, Hawker *et al.* reported the preparation of a donor–acceptor diblock copolymer, P3HT-*b*-DPP, comprising a poly(diketopyrrolopyrrole-terthiophene) (DPP)-based narrow bandgap block attached to a P3HT block.[117] A P3HT-*b*-DPP thin film annealed above the melting temperatures of both the P3HT and DPP crystallites self-assembled to form distinct lamellar structures with a domain spacing *d* of ~30 nm. Moreover, for the P3HT-*b*-DPP thin film, the crystallinity of each domain could be controlled by varying the annealing temperature. On the other hand, for the P3HT/DPP homopolymer blend film, gross macrophase separation was observed with no significant ordering. In the same year, Nakabayashi *et al.* reported a donor–acceptor–donor triblock copolymer, P3HT–PNBI–P3HT, composed of a poly(naphthalene diimide) (PNBI) mid-block and P3HT end blocks.[118] Devices were fabricated using a blend of the triblock copolymer with an added P3HT homopolymer (1 : 1 by weight). Annealing the blend film at 200 °C improved the magnitude of J_{SC} nearly three-fold, resulting in a PCE of 1.3%.

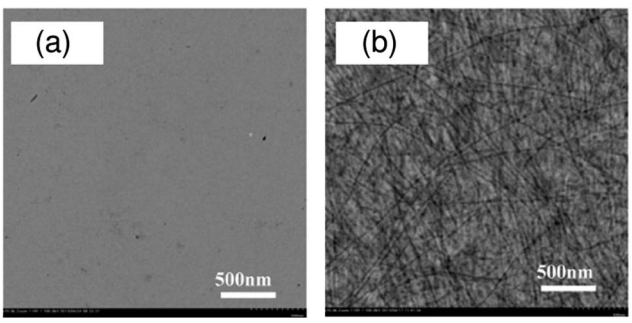

Fig. 20 Transmission electron microscopy images of the (a) P3HT/F8TBT blend film prepared from DCB and (b) P3HT-nanowire/F8TBT blend film prepared from a mixed solution of DCB and *n*-hexane. The scale bar corresponds to a length of 500 nm. All the blend films have a thickness of ~80 nm. Reproduced with permission from (ref. 53). Copyright 2014, American Chemical Society.

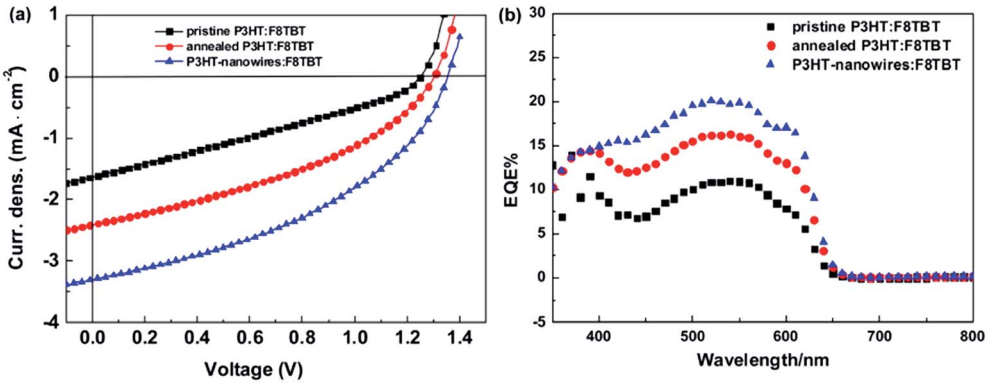

Fig. 21 (a) J–V characteristics and (b) EQE spectra of the as-cast P3HT/F8TBT (black squares), annealed P3HT/F8TBT (red circles), and P3HT-nanowire/F8TBT (blue triangles) blend solar cells under simulated AM1.5G solar light illumination with an intensity of 100 mW cm^{-2}. Both the annealed P3HT/F8TBT and P3HT-nanowire/F8TBT blends were annealed at 140 °C for 15 min before electrode deposition. Reproduced with permission from (ref. 53). Copyright 2014, American Chemical Society.

Independently, Higashihara *et al.* synthesized a donor–acceptor–donor triblock copolymer, P3HT–PNDITh–P3HT, composed of a poly(naphthalene diimide-*co*-thiophene) (PNDITh) mid-block and P3HT end blocks.[119] The triblock copolymer thin films were revealed to form a well-defined lamellar structure and crystalline domains for the respective blocks, where the P3HT layer was 10–20 nm thick and was aligned in an edge-on rich structure. In 2013, Verduzco *et al.* reported polymer solar cells based on donor–acceptor diblock copolymers consisting of poly(3-hexylthiophene)-*block*-poly [(9,9-dioctylfluorene)-2,7-diyl-*alt*-[4,7-bis(thiophene-5-yl)-2,1,3-benzothiadiazole]-2′,2″-diyl] (P3HT-*b*-PFTBT).[120] These block copolymers self-assembled to form in-plane lamellar structures with a d of ~18 nm, which is comparable to the typical exciton diffusion length (Fig. 23a). As a result, the optimally performing device based on the diblock polymer exhibited a PCE of 3.1%, which is higher than the PCE of 1.1% obtained for P3HT/F8TBT homopolymer blend solar cells (Fig. 23b). Although there is still significant room for improvement, steady progress has been made with regard to the synthesis and utilization of fully conjugated donor–acceptor block copolymers for all-polymer photovoltaics.

5. Morphology-limited free-carrier generation

Fig. 24 summarizes the maximum EQE values (EQE_{max}) reported for the polymer/polymer blend solar cells listed in Table 1. Apart from the various devices developed utilizing NDI-based polymers, the EQE_{max} values of the majority of the polymer/polymer blend solar cells are lower than 50%, irrespective of the donor/acceptor pair type. These EQE values are far below those that can be obtained for polymer/fullerene blend solar cells (70–90%).[3,4,6–8] The origin of such relatively low EQEs of polymer/polymer blends reported so far is generally attributed to the poor free charge-carrier generation capacity,[121–128] which seems to be inherent to the electronic structure of a donor/acceptor interface based on non-fullerene acceptors.

Ito *et al.* have investigated the efficiency for free charge-carrier generation in polymer/polymer blend solar cells based on P3HT and PF12TBT using TA measurements.[91] Note that the EQE_{max} of P3HT/PF12TBT blend solar cells has been limited to 30% to date,[91] while that of P3HT/PCBM blends has exceeded 80%.[4,5] Fig. 25 shows the charge generation and recombination dynamics for P3HT/PF12TBT blend films spin-coated from a CF solution and annealed at various temperatures for 10 min. As shown in this figure, the charge generation dynamics are characterized by immediate charge generation on a time scale determined by the pulse width of the excitation laser (~100 fs) and, also, subsequent delayed charge generation, which ends within a period of tens to hundreds of picoseconds, depending on the annealing temperature. The observation of immediate charge generation for all the blend films demonstrates that charge transfer (exciton dissociation) between P3HT and PF12TBT occurs so quickly that it does not limit the overall charge generation rate, as has been reported for polymer/PCBM blend films.[129–132] On the other hand, the delayed charge generation can be attributed to a diffusion controlled process; the rise time represents the time required for the polymer singlet exciton to reach the distributed donor/acceptor interface in the blends. In the as-spun (unannealed) blend film, polymer excitons were efficiently converted into charges with a rise time of 11 ps; however, the majority of the charges recombined geminately. Consequently, the generation efficiency of the long-lived free charge carriers (η_{Free}), which is defined as the ratio of the amount of the long-lived charge carriers to that of the overall generated charges, was as small as 36%. In the blend film annealed at 160 °C, on the other hand, the fraction of geminate recombination loss was reduced and, hence, η_{Free} increased up to 74%. For both blend films, the free charge carriers began to decay bimolecularly after a period of tens of nanoseconds. As illustrated in Fig. 26, the substantial charge loss due to geminate recombination in the as-spun blend film can be assigned to charges generated on isolated polymer chains in the matrix of the other polymer, and those generated at the finely mixed domain interface with disordered P3HT; these undesired blend morphologies hinder spatial separation

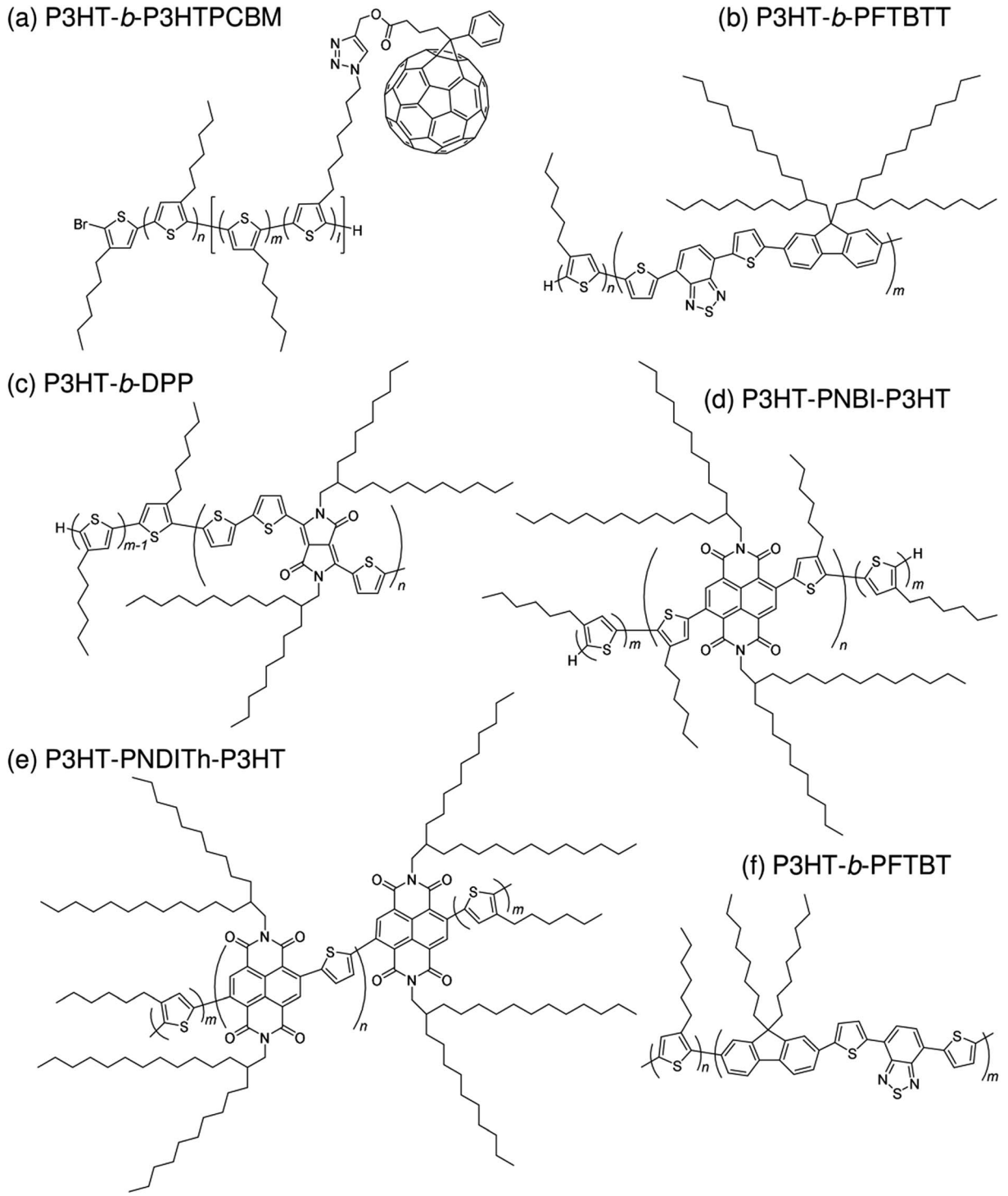

Fig. 22 Chemical structures of fully conjugated donor–acceptor block copolymers: (a) P3HT-*b*-P3HTPCBM; (b) P3HT-*b*-PFTBTT; (c) P3HT-*b*-DPP; (d) P3HT–PNBI–P3HT; (e) P3HT–PNDITh–P3HT; and (f) P3HT-*b*-PFTBT.

of the electron–hole pairs into free charges. Thermal annealing promotes demixing of the polymers, leading to the formation of relatively pure domains, ordering of the P3HT chains, and consequently, suppression of the geminate charge recombination. The results of TA measurements indicate that efficient generation of free charge carriers is not inherent to the polymer/fullerene interface, but it is possible for a polymer/polymer interface. In addition, the efficient free charge-carrier generation observed for P3HT/PF12TBT blend films indicates that crystalline polymer acceptors are not necessarily required for free carrier generation. Rather, the relatively low EQEs of polymer/polymer blend solar cells are due to the non-optimized blend morphology. This conclusion regarding efficient free charge-carrier generation at a polymer/polymer interface is

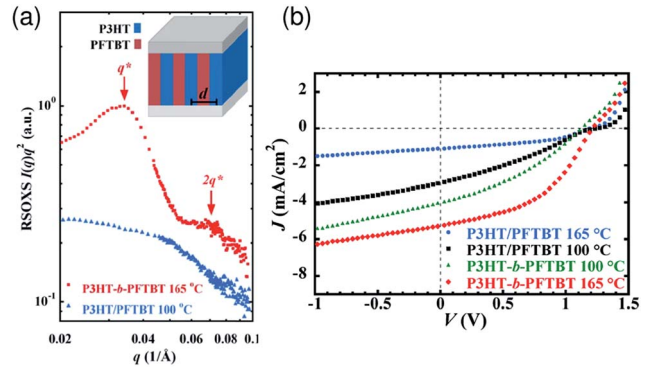

Fig. 23 (a) Resonant soft X-ray scattering intensities *versus* scattering vector of diblock copolymer P3HT-*b*-PFTBT and polymer blend P3HT/PFTBT (1 : 2 by mass) films in the transmission geometry. The P3HT-*b*-PFTBT and P3HT/PFTBT films were annealed at 165 °C and 100 °C, respectively. The q^* and $2q^*$ peaks of the block copolymer are indicative of lamellae. Inset: schematic illustration of P3HT-*b*-PFTBT films consisting of vertically oriented lamellae with average domain spacing labeled *d*. (b) *J*–*V* characteristics of diblock copolymer P3HT-*b*-PFTBT and polymer blend P3HT/PFTBT (1 : 2 by mass) solar cells annealed at different temperatures. The PCE of the block copolymer device is near 3%, whereas that of the blend device is 1%. Reproduced with permission from (ref. 120). Copyright 2013, American Chemical Society.

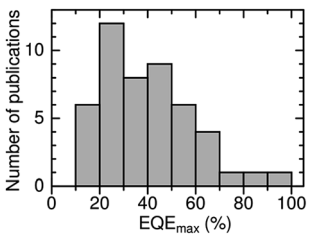

Fig. 24 Overall distribution of maximum EQE values reported for polymer/polymer blend solar cells listed in Table 1.

reinforced by the EQE_{max} values, which approach 70–90% for current, state-of-the-art polymer/polymer blend solar cells.

6. Outlook and challenges towards 10%

As a result of considerable research efforts expended on synthesizing various polymer acceptors and optimizing the blend morphology, the PCEs of polymer/polymer blend solar cells have improved significantly in recent years. However, the highest PCE remains below the PCE values of state-of-the-art polymer/fullerene blend solar cells, which have exceeded 10%. To further improve the PCEs of polymer/polymer blends, several challenges must be faced, including the developments of a pair of donor and acceptor polymers with high FF (even in the case of thick blend films), and a new photoactive layer design beyond the limit of simple donor/acceptor binary blends.

6.1 Ternary blends

The polymer/polymer blend solar cells with the highest level of PCEs reported in the recent literature have been fabricated by

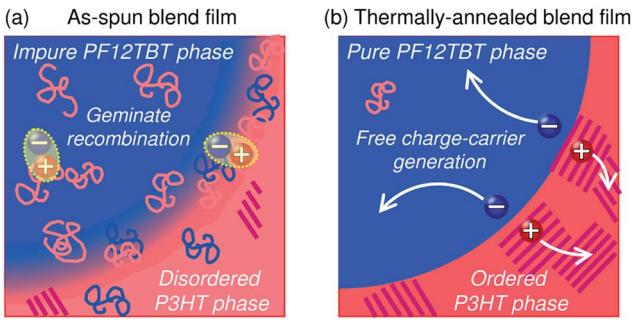

Fig. 26 Illustration of the nanoscale morphology of polymer phase separation; (a) the as-spun and (b) thermally annealed P3HT/PF12TBT blend films.

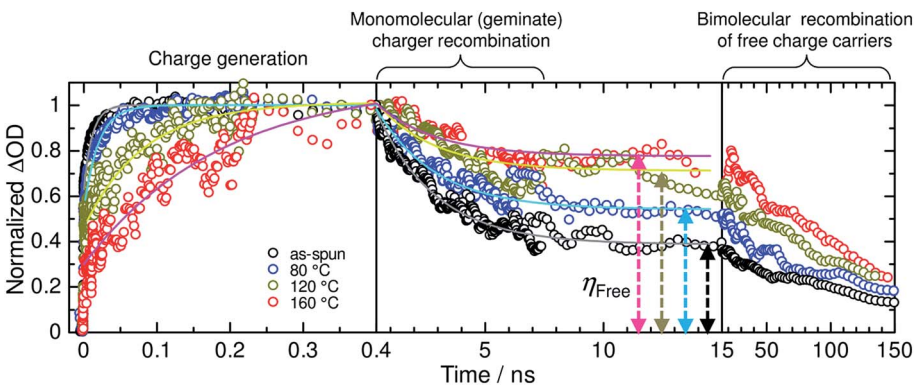

Fig. 25 Charge generation and recombination dynamics for the as-spun (black circles) and annealed P3HT/PF12TBT blend films at 80, 120, and 160 °C (blue, gold, and red circles, respectively) for 10 min. The TA signals for the charge-induced absorption (ΔOD) were normalized, with the maximum peak intensities set to 1. The solid lines represent the best fitting curves obtained using $\Delta OD(t) = A[1 - \exp(-t/\tau_R)] + B$ for the charge generation dynamics and $\Delta OD(t) = G\exp(-t/\tau_D) + C$ for the charge recombination dynamics. η_{Free}, which is defined as $C/(G + C)$, was increased *via* thermal annealing from 36% (as-spun film) to 51% (80 °C-annealed film), 67% (120 °C-annealed film), and 74% (160 °C-annealed film). Reproduced with permission from (ref. 91). Copyright 2015, Wiley-VCH Verlag GmbH & Co. KGaA, Weinheim.

blending a pair of low-bandgap donor and acceptor polymers that exhibit efficient light-absorption capabilities at near-IR wavelengths. This is important in order to obtain large J_{SC} values, even when the thin films optimal for charge-carrier collection are employed. On the other hand, the combination of such low-bandgap polymers inevitably results in weak light absorptivity in the visible region, owing to the intrinsic narrow absorption bandwidths of organic semiconductors (see Fig. 13b). Therefore, further improvement in the PCE requires new design strategies that can complement the weak absorption in the visible range. Ternary blend solar cells, which are fabricated by blending a third material (polymer donor, fullerene acceptor, or dye molecule) into a binary blend of a polymer donor and a PCBM acceptor, are emerging as a fascinating approach to broadening the absorption bandwidth of the photoactive layer.[133–139]

In 2015, Jenekhe *et al.* fabricated ternary blend all-polymer solar cells composed of one polymer donor PBDTTT-C-T, and two polymer acceptors, naphthalene diimide–selenophene (PNDIS-HD) copolymer and perylene diimide–selenophene (PPDIS) copolymer.[140] A PDTTT-CT/PNDIS-HD/PPDIS (1 : 0.25 : 0.75 by weight) ternary blend exhibited a PCE of 3.2%, which is enhanced compared with those of the corresponding PDTTT-CT/PNDIS-HD (PCE of 1.3%) and PDTTT-CT/PPDIS (PCE of 2.1%) binary blend solar cells. As shown in Fig. 27, the J_{SC} as well as the EQE spectrum of the optimal ternary blend are almost equal to the sum of those of the two binary blends. From analysis of the composition dependence of the photovoltaic parameters, Jenekhe *et al.* proposed a parallel-like BHJ as a working mechanism for the ternary blend systems.

Also in 2015, Ito *et al.* designed ternary blend all-polymer solar cells in which a wide-bandgap polymer, PCDTBT, was introduced into the low-bandgap PTB7-Th/P(NDI2OD-T2) blend as a second donor (Fig. 28).[141] For a ternary blend all-polymer solar cell containing 10-wt% PCDTBT, the relatively low EQEs at visible wavelengths of the PTB7-Th/P(NDI2OD-T2) binary blend were increased from 50% to *ca.* 70%, while retaining the excellent EQEs of ~60% at near-IR wavelengths (Fig. 28c). Consequently, a PCE of 6.65% with a J_{SC} of 14.4 mA cm^{-2} was achieved, which is significantly higher than the value of 5.70% with a J_{SC} of 12.4 mA cm^{-2} obtained for an individually optimized PTB7-Th/P(NDI2OD-T2) binary blend. The compositional dependence strongly suggests that PCDTBT contributed to the photocurrent generation as a visible sensitizer through efficient energy transfer for both PTB7-Th and P(NDI2OD-T2). In that case, the PCDTBT absorbed visible light, but relied on both PBDTTT-EF-T and N2200 host polymers to generate and transport free charge carriers. Thus, an improvement in the PCE can be achieved by taking full advantage of the excellent photovoltaic conversion characteristics of the PTB7-Th/P(NDI2OD-T2) binary blend.[61] Ito *et al.*'s results suggest that the use of ternary blends composed of a wide-bandgap polymer as a third material, along with an efficient low-bandgap donor/acceptor polymer blend, is an effective strategy for achieving higher-efficiency all-polymer blend solar cells. We note that, as predicted by the broken line in Fig. 3a, a PCE of close to 10% can be achieved if J_{SC} is improved to more than 22 mA cm^{-2}. Such a target J_{SC} value will be achievable by applying the concept of ternary blends to the state-of-the-art low-bandgap PTB7-Th/PNDIS-HD blends that suffer from weak light absorptivity in the visible range (see Fig. 13b).

6.2 Suppression of bimolecular charge recombination for high FF

The superior performance of polymer/fullerene blend solar cells has been attributed not only to the large J_{SC} approaching 18 mA cm^{-2}, but also to the high FFs of larger than 0.7, which are obtained at the same time.[6–9] However, the majority of polymer/polymer blend solar cells reported to date exhibit FFs of less than 0.6 (Fig. 3c). Even the current, state-of-the-art devices with the highest level of PCEs are affected by the same problem, which suggests that the FF is the primary factor limiting the PCEs of the present polymer/polymer blend solar cells. For example, PBDTTT-C-T/30PDI blend solar cells have exhibited a PCE of 6.29% with a FF of 0.45,[74] and PTB7-Th/PNDIS-HD blends have yielded a PCE of 7.73% with a FF of 0.51.[76] If the FF of these blend systems could be improved to 0.70, PCEs of 10% could be obtained.

It is widely believed that, in order to achieve high FF in polymer/fullerene blend solar cells, the μ_h and μ_e should be balanced and greater than 10^{-4} cm^2 V^{-1} s^{-1}. With regard to this point, the FF values of polymer/polymer blend solar cells based

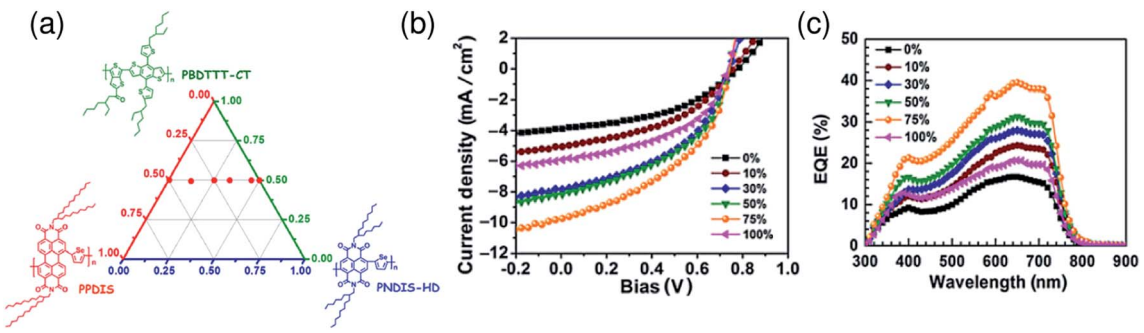

Fig. 27 (a) Composition of the ternary [PBDTTT-C-T]$_1$[PNDIS-HD]$_{1-x}$[PPDIS]$_x$ blend illustrated on a ternary diagram. (b) *J*–*V* characteristics and (c) EQE spectra as functions of [PPDIS]$_x$ composition, where *x* is the PPDIS weight fraction in the binary acceptor components (x = 0.10, 0.30, 0.50, 0.75). Reproduced with permission from (ref. 140). Copyright 2015, Materials Research Society.

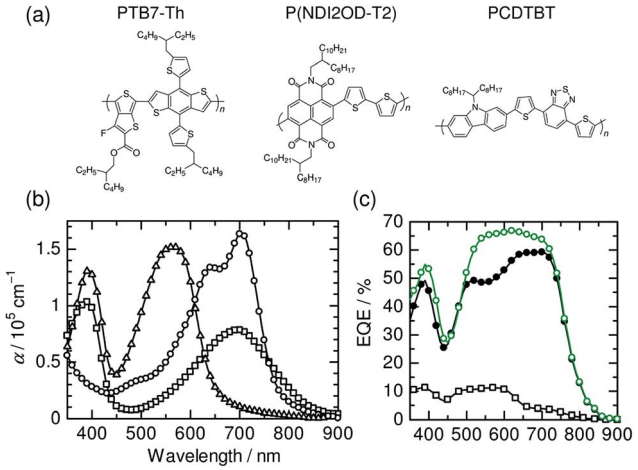

Fig. 28 (a) Chemical structures of polymers used for ternary blend solar cells. (b) Absorption coefficients α of PTB7-Th (circles), P(NDI2OD-T2) (squares), and PCDTBT (triangles) measured in neat films. (c) EQE spectra of PTB7-Th/P(NDI2OD-T2)/PCDTBT ternary (open circles), PTB7-Th/P(NDI2OD-T2) binary (solid circles), and P(NDI2OD-T2)/N2200 binary (open squares) BHJ solar cells measured under AM1.5G illumination from a calibrated solar simulator with 100 mW cm^{-2} intensity. The loading amount of PCDTBT in the ternary blend was 10 wt%. Reproduced with permission from (ref. 141). Copyright 2015, The Royal Society of Chemistry.

on rylene diimide-based polymer acceptors in Table 1 have been plotted against the μ_h and μ_e in such blends in Fig. 29a and b. In addition, the mobility ratio of two carriers for each device, which is defined as the ratio of the slower carrier mobility to the faster carrier mobility, has been calculated and plotted against the corresponding FF (Fig. 29c). These plots illustrate that the FFs are limited to approximately 0.6, even for devices with high mobility values (>10^{-4} cm^2 V^{-1} s^{-1}) and balanced mobility ratios (>0.1). In other words, establishing such relatively high and balanced mobilities alone is not sufficient to obtain an excellent FF approaching 0.7. Recent studies by Neher *et al.*,[54] Koster *et al.*,[142] and McGehee *et al.*[143] suggest that this is because the FF does not depend on the charge extraction rate only; rather, it can be determined by the ratio of the extraction and recombination rates of the charge carriers. To achieve high FFs in polymer/polymer blend systems, it is important to reduce the bimolecular recombination of charge carriers, in addition to improving the charge transport ability of constituent polymers by establishing high and balanced mobilities.

Among the polymer/polymer blend solar cells reported to date, only a few sets of semicrystalline polymer/polymer blends, J51/P(NDI2OD-T2), P3HT/P(NDI2OD-T2) and P3HT/P(NDI-TCPDTT), can function with excellent FF values of 0.65–0.70. Interestingly, as shown by the stars in Fig. 29d, P3HT/P(NDI2OD-T2) and P3HT/P(NDI-TCPDTT) blends maintain excellent FFs even for thick active layers of more than 300 nm.[44,54] Neher *et al.* have ascribed the high FF of the P3HT/P(NDI2OD-T2) blend to the strongly suppressed bimolecular recombination coefficient γ_{BMR}, which is as small as 5×10^{-12} cm^3 s^{-1}. This γ_{BMR} is a factor of 1000 lower than the Langevin-type recombination coefficient γ_L of 3×10^{-9} cm^3 s^{-1}, as obtained from eqn (2) using the carrier mobilities measured for the blend:[54]

$$\gamma_L = \frac{q}{\varepsilon_0 \varepsilon_R}(\mu_h + \mu_e) \quad (2)$$

where q is the elementary charge, ε_0 is the vacuum permittivity, and ε_R is the relative permittivity of the active layer. Further, Neher *et al.* have suggested that the reduced bimolecular recombination is achieved *via* the use of the optimum blend morphology characterized by high polymer crystallinity combined with sufficiently pure polymer domains. Neher *et al.*'s experimental results indicate the considerable potential for achieving FF of 0.7 by controlling the blend morphology, even for other combinations of semicrystalline donor and acceptor polymers. This finding will stimulate further research efforts towards the development of new polymers and morphology control techniques, with a view to achieving 10% PCE in polymer/polymer blend solar cells.

7. Conclusion

The ongoing developments of NDI-based polymer acceptors and the continuous efforts towards controlling the blend morphology have increased the PCEs of polymer/polymer blend solar cells above the 8% level. In particular, state-of-the-art low-bandgap donor/acceptor blends have exhibited maximum EQEs exceeding 80%, indicating that both the generation and collection efficiencies of the free charge carriers are higher than 80% under short-circuit conditions. These results confirm that

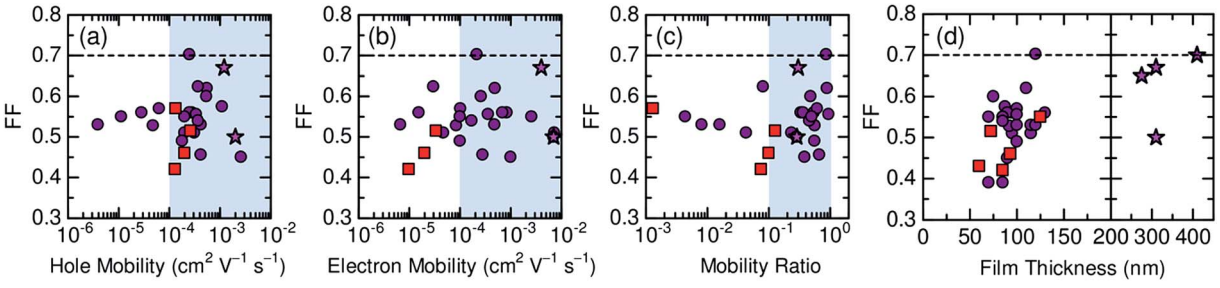

Fig. 29 Plots of (a) hole and (b) electron mobilities measured in the blend film *versus* FF measured in solar cells composed of PDI-based (squares) and NDI-based (circles and stars) polymer acceptors. (c) Mobility ratio, defined as the ratio of the slower carrier mobility to the faster carrier mobility, *versus* corresponding FF. (d) Plots of device film thickness *versus* corresponding FF.

the capacity for efficient free charge-carrier generation is not inherent to the polymer/fullerene domain interface, but it is possible for a polymer/polymer domain interface. On the other hand, further improvement of these devices towards the achievement of 10% PCE requires sufficient light absorption at visible wavelengths and a high FF close to 0.7. Broadening the absorption bandwidth through a ternary blend of conjugated polymers and reducing the bimolecular charge recombination by optimizing the blend morphology will pave the way towards the realization of 10% PCE for these devices.

Acknowledgements

This work was supported by the Japan Society for the Promotion of Science (JSPS) through the "Funding Program for World-Leading Innovative R&D on Science and Technology (FIRST Program)," initiated by the Council for Science and Technology Policy (CSTP), the CREST program from the Japan Science and Technology Agency, and the JSPS KAKENHI Grant Number 26288060.

References

1 R. Søndergaard, M. Hösel, D. Angmo, T. T. Larsen-Olsen and F. C. Krebs, *Mater. Today*, 2012, **15**, 36.
2 S. B. Darling and F. You, *RSC Adv.*, 2013, **3**, 17633.
3 L. Bian, E. Zhu, J. Tang, W. Tang and F. Zhang, *Prog. Polym. Sci.*, 2012, **37**, 1292.
4 C. J. Brabec, S. Gowrisanker, J. J. M. Halls, D. Laird, S. Jia and S. P. Williams, *Adv. Mater.*, 2010, **22**, 3839.
5 G. Dennler, M. C. Scharber and C. J. Brabec, *Adv. Mater.*, 2009, **21**, 1323.
6 V. Vohra, K. Kawashima, T. Kakara, T. Koganezawa, I. Osaka, K. Takimiya and H. Murata, *Nat. Photonics*, 2015, **9**, 403.
7 Z. He, B. Xiao, F. Liu, H. Wu, Y. Yang, S. Xiao, C. Wang, T. P. Russell and Y. Cao, *Nat. Photonics*, 2015, **9**, 174.
8 Y. Liu, J. Zhao, Z. Li, C. Mu, W. Ma, H. Hu, K. Jiang, H. Lin, H. Ade and H. Yan, *Nat. Commun.*, 2014, **5**, 5293.
9 M. A. Green, K. Emery, Y. Hishikawa, W. Warta and E. D. Dunlop, *Prog. Photovolt. Res. Appl.*, 2016, **24**, 3.
10 S. C. Veenstra, J. Loos and J. M. Kroon, *Prog. Photovolt. Res. Appl.*, 2007, **15**, 727.
11 C. R. McNeill and N. C. Greenham, *Adv. Mater.*, 2009, **21**, 3840.
12 C. R. McNeill, *Energy Environ. Sci.*, 2012, **5**, 5653.
13 A. Facchetti, *Mater. Today*, 2013, **16**, 123.
14 T. Kim, J. H. Kim, T. E. Kang, C. Lee, H. Kang, M. Shin, C. Wang, B. Ma, U. Jeong, T. S. Kim and B. J. Kim, *Nat. Commun.*, 2015, **6**, 8547.
15 P. J. Flory, *Principles of Polymer Chemistry*, Cornell University Press, 1953, pp. 495–540.
16 G. Strobl, *The Physics of Polymers—Concepts for Understanding Their Structures and Behavior*, Springer-Verlag, Berlin Heidelberg, 3rd rev. and expanded edn, 2007, pp. 106–122.
17 O. V. Mikhnenko, H. Azimi, M. Scharber, M. Morana, P. W. M. Blom and M. A. Loi, *Energy Environ. Sci.*, 2012, **5**, 6960.
18 O. V. Mikhnenko, P. W. M. Blom and T.-Q. Nguyen, *Energy Environ. Sci.*, 2015, **8**, 1867.
19 Y. Wang, H. Benten, S. Ohara, D. Kawamura, H. Ohkita and S. Ito, *ACS Appl. Mater. Interfaces*, 2014, **6**, 14108.
20 Y. Tamai, Y. Matsuura, H. Ohkita, H. Benten and S. Ito, *J. Phys. Chem. Lett.*, 2014, **5**, 399.
21 Y. Tamai, H. Ohkita, H. Benten and S. Ito, *J. Phys. Chem. Lett.*, 2015, **6**, 3417.
22 T. M. Clarke and J. R. Durrant, *Chem. Rev.*, 2010, **110**, 6736.
23 H. Ohkita and S. Ito, *Polymer*, 2011, **52**, 4397.
24 H. Ohkita and S. Ito, *Organic Solar Cells—Materials and Device Physics—*, ed. W. C. H. Choy, Springer-Verlag, London, 2013, pp. 103–137.
25 H. Ohkita, Y. Tamai, H. Benten and S. Ito, *IEEE J. Sel. Top. Quantum Electron.*, 2016, **22**, 4100612.
26 J. J. M. Halls, C. A. Walsh, N. C. Greenham, E. A. Marseglia, R. H. Friend, S. C. Moratti and A. B. Holmes, *Nature*, 1995, **376**, 498.
27 G. Yu and A. J. Heeger, *J. Appl. Phys.*, 1995, **78**, 4510.
28 M. Granström, K. Petritsch, A. C. Arias, A. Lux, M. R. Andersson and R. H. Friend, *Nature*, 1998, **395**, 257.
29 A. J. Breeze, Z. Schlesinger, S. A. Carter, H. Tillmann and H.-H. Hörhold, *Sol. Energy Mater. Sol. Cells*, 2004, **83**, 263.
30 T. Kietzke, H.-H. Hörhold and D. Neher, *Chem. Mater.*, 2005, **17**, 6532.
31 M. M. Koetse, J. Sweelssen, K. T. Hoekerd, H. F. M. Schoo, S. C. Veenstra, J. M. Kroon, X. Yang and J. Loos, *Appl. Phys. Lett.*, 2006, **88**, 083504.
32 X. Zhan, Z. Tan, B. Domercq, Z. An, X. Zhang, S. Barlow, Y. Li, D. Zhu, B. Kippelen and S. R. Marder, *J. Am. Chem. Soc.*, 2007, **129**, 7246.
33 C. R. McNeill, A. Abrusci, J. Zaumseil, R. Wilson, M. J. McKieman, J. H. Burroughes, J. J. M. Halls, N. C. Greenham and R. H. Friend, *Appl. Phys. Lett.*, 2007, **90**, 193506.
34 Z. Tan, E. Zhou, X. Zhan, X. Wang, Y. Li, S. Barlow and S. R. Marder, *Appl. Phys. Lett.*, 2008, **93**, 073309.
35 G. Sang, Y. Zou, Y. Huang, G. Zhao, Y. Yang and Y. Li, *Appl. Phys. Lett.*, 2009, **94**, 193302.
36 T. W. Holcombe, C. H. Woo, D. F. J. Kavulak, B. C. Thompson and J. M. J. Fréchet, *J. Am. Chem. Soc.*, 2009, **131**, 14160.
37 J. A. Mikroyannidis, M. M. Stylianakis, G. D. Sharma, P. Balraju and M. S. Roy, *J. Phys. Chem. C*, 2009, **113**, 7904.
38 X. He, F. Gao, G. Tu, D. Hasko, S. Hüttner, U. Steiner, N. C. Greenham, R. H. Friend and W. T. S. Huck, *Nano Lett.*, 2010, **10**, 1302.
39 S. Fabiano, Z. Chen, S. Vahedi, A. Facchetti, B. Pignataro and M. A. Loi, *J. Mater. Chem.*, 2011, **21**, 5891.
40 T. W. Holcombe, J. E. Norton, J. Rivnay, C. H. Woo, L. Goris, C. Piliego, G. Griffini, A. Sellinger, J.-L. Brédas, A. Salleo and J. M. J. Fréchet, *J. Am. Chem. Soc.*, 2011, **133**, 12106.
41 D. Mori, H. Benten, J. Kosaka, H. Ohkita, S. Ito and K. Miyake, *ACS Appl. Mater. Interfaces*, 2011, **3**, 2924.

42 E. Zhou, J. Cong, Q. Wei, K. Tajima, C. Yang and K. Hashimoto, *Angew. Chem., Int. Ed.*, 2011, **50**, 2799.
43 Y.-J. Hwang, G. Ren, N. M. Murari and S. A. Jenekhe, *Macromolecules*, 2012, **45**, 9056.
44 M. Schubert, D. Dolfen, J. Frisch, S. Roland, R. Steyrleuthner, B. Stiller, Z. Chen, U. Scherf, N. Koch, A. Facchetti and D. Neher, *Adv. Energy Mater.*, 2012, **2**, 369.
45 E. Zhou, J. Cong, M. Zhao, L. Zhang, K. Hashimoto and K. Tajima, *Chem. Commun.*, 2012, **48**, 5283.
46 D. Mori, H. Benten, H. Ohkita, S. Ito and K. Miyake, *ACS Appl. Mater. Interfaces*, 2012, **4**, 3325.
47 Y. Tang and C. R. McNeill, *J. Polym. Sci., Part B: Polym. Phys.*, 2013, **51**, 403.
48 Y. Zhou, Q. Yan, Y.-Q. Zheng, J.-Y. Wang, D. Zhao and J. Pei, *J. Mater. Chem. A*, 2013, **1**, 6609.
49 T. Earmme, Y. J. Hwang, N. M. Murari, S. Subramaniyan and S. A. Jenekhe, *J. Am. Chem. Soc.*, 2013, **135**, 14960.
50 E. Zhou, J. Cong, K. Hashimoto and K. Tajima, *Adv. Mater.*, 2013, **25**, 6991.
51 D. Mori, H. Benten, I. Okada, H. Ohkita and S. Ito, *Adv. Energy Mater.*, 2014, **4**, 1301006.
52 Q. Yang, H. Song, B. Gao, Y. Wang, Y. Fu, J. Yang, Z. Xie and L. Wang, *RSC Adv.*, 2014, **4**, 12579.
53 W. Yu, D. Yang, X. Zhu, X. Wang, G. Tu, D. Fan, J. Zhang and C. Li, *ACS Appl. Mater. Interfaces*, 2014, **6**, 2350.
54 S. Roland, M. Schubert, B. A. Collins, J. Kurpiers, Z. Chen, A. Facchetti, H. Ade and D. Neher, *J. Phys. Chem. Lett.*, 2014, **5**, 2815.
55 N. Zhou, H. Lin, S. J. Lou, X. Yu, P. Guo, E. F. Manley, S. Loser, P. Hartnett, H. Huang, M. R. Wasielewski, L. X. Chen, R. P. H. Chang, A. Facchetti and T. J. Marks, *Adv. Energy Mater.*, 2014, **4**, 1300785.
56 P. Cheng, L. Ye, X. Zhao, J. Hou, Y. Li and X. Zhan, *Energy Environ. Sci.*, 2014, **7**, 1351.
57 Y. Zhou, T. Kurosawa, W. Ma, Y. Guo, L. Fang, K. Vandewal, Y. Diao, C. Wang, Q. Yan, J. Reinspach, J. Mei, A. L. Appleton, G. I. Koleilat, Y. Gao, S. C. B. Mannsfeld, A. Salleo, H. Ade, D. Zhao and Z. Bao, *Adv. Mater.*, 2014, **26**, 3767.
58 H. Kang, K.-H. Kim, J. Choi, C. Lee and B. J. Kim, *ACS Macro Lett.*, 2014, **3**, 1009.
59 T. Earmme, Y.-J. Hwang, S. Subramaniyan and S. A. Jenekhe, *Adv. Mater.*, 2014, **26**, 6080.
60 C. Mu, P. Liu, W. Ma, K. Jiang, J. Zhao, K. Zhang, Z. Chen, Z. Wei, Y. Yi, J. Wang, S. Yang, F. Huang, A. Facchetti, H. Ade and H. Yan, *Adv. Mater.*, 2014, **26**, 7224.
61 D. Mori, H. Benten, I. Okada, H. Ohkita and S. Ito, *Energy Environ. Sci.*, 2014, **7**, 2939.
62 G. Shi, J. Yuan, X. Huang, Y. Lu, Z. Liu, J. Peng, G. Ding, S. Shi, J. Sun, K. Lu, H.-Q. Wang and W. Ma, *J. Phys. Chem. C*, 2015, **119**, 25298.
63 B. Xiao, G. Ding, Z. Tan and E. Zhou, *Polym. Chem.*, 2015, **6**, 7594.
64 S. Dai, P. Cheng, Y. Lin, Y. Wang, L. Ma, Q. Ling and X. Zhan, *Polym. Chem.*, 2015, **6**, 5254.
65 F. Liu, H. Li, C. Gu and H. Fu, *RSC Adv.*, 2015, **5**, 10072.
66 L. Ye, X. Jiao, H. Zhang, S. Li, H. Yao, H. Ade and J. Hou, *Macromolecules*, 2015, **48**, 7156.
67 W. Li, Y. An, M. M. Wienk and R. A. J. Janssen, *J. Mater. Chem. A*, 2015, **3**, 6756.
68 I. H. Jung, D. Zhao, J. Jang, W. Chen, E. S. Landry, L. Lu, D. V. Talapin and L. Yu, *Chem. Mater.*, 2015, **27**, 5941.
69 F. Liu, H. Li, Y. Wu, C. Gu and H. Fu, *RSC Adv.*, 2015, **5**, 92151.
70 J. Yuan and W. Ma, *J. Mater. Chem. A*, 2015, **3**, 7077.
71 H. Kang, M. A. Uddin, C. Lee, K.-H. Kim, T. L. Nguyen, W. Lee, Y. Li, C. Wang, H. Y. Woo and B. J. Kim, *J. Am. Chem. Soc.*, 2015, **137**, 2359.
72 L. Ye, X. Jiao, M. Zhou, S. Zhang, H. Yao, W. Zhao, A. Xia, H. Ade and J. Hou, *Adv. Mater.*, 2015, **27**, 6046.
73 C. Lee, H. Kang, W. Lee, T. Kim, K. H. Kim, H. Y. Woo, C. Wang and B. J. Kim, *Adv. Mater.*, 2015, **27**, 2466.
74 Y. J. Hwang, T. Earmme, B. A. E. Courtright, F. N. Eberle and S. A. Jenekhe, *J. Am. Chem. Soc.*, 2015, **137**, 4424.
75 J. W. Jung, J. W. Jo, C. C. Chueh, F. Liu, W. H. Jo, T. P. Russell and A. K.-Y. Jen, *Adv. Mater.*, 2015, **27**, 3310.
76 Y. J. Hwang, B. A. E. Courtright, A. S. Ferreira, S. H. Tolbert and S. A. Jenekhe, *Adv. Mater.*, 2015, **27**, 4578.
77 L. Gao, Z.-G. Zhang, L. Xue, J. Min, J. Zhang, Z. Wei and Y. Li, *Adv. Mater.*, 2016, **28**, 1884.
78 H. Yan, Z. Chen, Y. Zheng, C. Newman, J. R. Quinn, F. Dötz, M. Kastler and A. Facchetti, *Nature*, 2009, **457**, 679.
79 J. R. Moore, S. Albert-Seifried, A. Rao, S. Massip, B. Watts, D. J. Morgan, R. H. Friend, C. R. McNeill and H. Sirringhaus, *Adv. Energy Mater.*, 2011, **1**, 230.
80 H. Yan, B. A. Collins, E. Gann, C. Wang, H. Ade and C. R. McNeill, *ACS Nano*, 2012, **6**, 677.
81 R. Steyrleuthner, M. Schubert, I. Howard, B. Klaumünzer, K. Schilling, Z. Chen, P. Saalfrank, F. Laquai, A. Facchetti and D. Neher, *J. Am. Chem. Soc.*, 2012, **134**, 18303.
82 http://faculty.wcas.northwestern.edu/∼afa912/.
83 A. C. Arias, J. D. MacKenzie, R. Stevenson, J. J. H. Halls, M. Inbasekaran, E. P. Woo, D. Richards and R. H. Friend, *Macromolecules*, 2001, **34**, 6005.
84 H. J. Snaith, A. C. Arias, A. C. Morteani, C. Silva and R. H. Friend, *Nano Lett.*, 2002, **2**, 1353.
85 R. Shikler, M. Chiesa and R. H. Friend, *Macromolecules*, 2006, **39**, 5393.
86 S. Swaraj, C. Wang, H. Yan, B. Watts, J. Lüning, C. R. McNeill and H. Ade, *Nano Lett.*, 2010, **10**, 2863.
87 C. R. McNeill, A. Abrusci, I. Hwang, M. A. Ruderer, R. M. Buschbaum and N. C. Greenham, *Adv. Funct. Mater.*, 2009, **19**, 3103.
88 H. C. Liao, C. C. Ho, C. Y. Chang, M. H. Jao, S. B. Darling and W. F. Su, *Mater. Today*, 2013, **16**, 326.
89 X. Liu, S. Huettner, Z. Rong, M. Sommer and R. H. Friend, *Adv. Mater.*, 2012, **24**, 669.
90 S. Ito, T. Hirata, D. Mori, H. Benten, L. T. Lee and H. Ohkita, *J. Photopolym. Sci. Technol.*, 2013, **26**, 175.
91 D. Mori, H. Benten, H. Ohkita and S. Ito, *Adv. Energy Mater.*, 2015, **5**, 1500304.
92 S. R. Scully, P. B. Armstrong, C. Edder, J. M. J. Fréchet and M. D. McGehee, *Adv. Mater.*, 2007, **19**, 2961.

93 Y. Wang, H. Ohkita, H. Benten and S. Ito, *ChemPhysChem*, 2015, **16**, 1263.
94 J. K. J. van Duren, X. Yang, J. Loos, C. W. T. Bulle-Lieuwma, A. B. Sieval, J. C. Hummelen and R. A. J. Janssen, *Adv. Funct. Mater.*, 2004, **14**, 425.
95 L. M. Andersson, F. Zhang and O. Inganäs, *Appl. Phys. Lett.*, 2007, **91**, 071108.
96 S. Wakim, S. Beaupré, N. Blouin, B. Aich, S. Rodman, R. Gaudiana, Y. Tao and M. Leclerc, *J. Mater. Chem.*, 2009, **19**, 5351.
97 S. Berson, R. D. Bettignies, S. Bailly and S. Guillerez, *Adv. Funct. Mater.*, 2007, **17**, 1377.
98 H. Xin, G. Ren, F. S. Kim and S. A. Jenekhe, *Chem. Mater.*, 2008, **20**, 6199.
99 Z. Yin and Q. Zheng, *Adv. Energy Mater.*, 2012, **2**, 179.
100 S. B. Jo, W. H. Lee, L. Qiu and K. Cho, *J. Mater. Chem.*, 2012, **22**, 4244.
101 T. Salim, S. Sun, L. H. Wong, L. Xi, Y. L. Foo and Y. M. Lam, *J. Phys. Chem. C*, 2010, **114**, 9459.
102 S. Samitsu, T. Shimomura and K. Ito, *Thin Solid Films*, 2008, **516**, 2478.
103 C. R. G. Grenier, W. Pisula, T. J. Joncheray, K. Müllen and J. R. Reynolds, *Angew. Chem., Int. Ed.*, 2007, **46**, 714.
104 H.-W. Wang, E. Pentzer, T. Emrick and T. P. Russell, *ACS Macro Lett.*, 2014, **3**, 30.
105 A. L. Briseno, S. C. B. Mannsfeld, P. J. Shamberger, F. S. Ohuchi, Z. Bao, S. A. Jenekhe and Y. Xia, *Chem. Mater.*, 2008, **20**, 4712.
106 E. V. Canesi, A. Luzio, B. Saglio, A. Bianco, M. Caironi and C. Bertarelli, *ACS Macro Lett.*, 2012, **1**, 366.
107 F. S. Bates and G. H. Fredrickson, *Annu. Rev. Phys. Chem.*, 1990, **41**, 525.
108 F. S. Bates, *Science*, 1991, **251**, 898.
109 P. F. van Hutten and G. Hadziioannou, *Monatsh. Chem.*, 2001, **132**, 129.
110 U. Stalmach, B. de Boer, C. Videlot, P. F. van Hutten and G. Hadziioannou, *J. Am. Chem. Soc.*, 2000, **122**, 5464.
111 M. J. Robb, S.-Y. Ku and C. J. Hawker, *Adv. Mater.*, 2013, **25**, 5686.
112 J. Wang and T. Higashihara, *Polym. Chem.*, 2013, **4**, 5518.
113 K. Nakabayashi and H. Mori, *Materials*, 2014, **7**, 3274.
114 Y. Lee and E. D. Gomez, *Macromolecules*, 2015, **48**, 7385.
115 S. Miyanishi, Y. Zhang, K. Tajima and K. Hashimoto, *Chem. Commun.*, 2010, **46**, 6723.
116 R. C. Mulherin, S. Jung, S. Huettner, K. Johnson, P. Kohn, M. Sommer, S. Allard, U. Scherf and N. C. Greenham, *Nano Lett.*, 2011, **11**, 4846.
117 S.-Y. Ku, M. A. Brady, N. D. Treat, J. E. Cochran, M. J. Robb, E. J. Kramer, M. L. Chabinyc and C. J. Hawker, *J. Am. Chem. Soc.*, 2012, **134**, 16040.
118 K. Nakabayashi and H. Mori, *Macromolecules*, 2012, **45**, 9618.
119 J. Wang, M. Ueda and T. Higashihara, *ACS Macro Lett.*, 2013, **2**, 506.
120 C. Guo, Y.-H. Lin, M. D. Witman, K. A. Smith, C. Wang, A. Hexemer, J. Strzalka, E. D. Gomez and R. Verduzco, *Nano Lett.*, 2013, **13**, 2957.
121 C. Yin, T. Kietzke, M. Kumke, D. Neher and H.-H. Hörhold, *Sol. Energy Mater. Sol. Cells*, 2007, **91**, 411.
122 C. Yin, M. Schubert, S. Bange, B. Stiller, M. Castellani, D. Neher, M. Kumke and H.-H. Hörhold, *J. Phys. Chem. C*, 2008, **112**, 14607.
123 M. M. Mandoc, W. Veurman, L. J. A. Koster, B. Boer and P. W. M. Blom, *Adv. Funct. Mater.*, 2007, **17**, 2167.
124 A. G. Rabade, A. C. Morteani and R. H. Friend, *Adv. Mater.*, 2009, **21**, 3924.
125 J. M. Hodgkiss, A. R. Campbell, R. A. Marsh, A. Rao, S. A. Seifried and R. H. Friend, *Phys. Rev. Lett.*, 2010, **104**, 177701.
126 C. R. McNeill, S. Westenhoff, C. Groves, R. H. Friend and N. C. Greenham, *J. Phys. Chem. C*, 2007, **111**, 19153.
127 Y.-S. Huang, S. Westenhoff, I. Avilov, P. Sreearunothai, J. M. Hodgkiss, C. Deleener, R. H. Friend and D. Beljonne, *Nat. Mater.*, 2008, **7**, 483.
128 C. Groves, R. A. Marsh and N. C. Greenham, *J. Chem. Phys.*, 2008, **129**, 114903.
129 J. Guo, H. Ohkita, H. Benten and S. Ito, *J. Am. Chem. Soc.*, 2010, **132**, 6154.
130 I. A. Howard, R. Mauer, M. Meister and F. Laquai, *J. Am. Chem. Soc.*, 2010, **132**, 14866.
131 C. J. Brabec, G. Zerza, G. Cerullo, S. D. Silvestri, S. Luzzati, J. C. Hummelen and S. Sariciftci, *Chem. Phys. Lett.*, 2001, **340**, 232.
132 S. Yamamoto, H. Ohkita, H. Benten, S. Ito, S. Yamamoto, D. Kitazawa and J. Tsukamoto, *J. Phys. Chem. C*, 2013, **117**, 11514.
133 Q. An, F. Zhang, J. Zhang, W. Tang, Z. Deng and B. Hu, *Energy Environ. Sci.*, 2016, **9**, 281.
134 L. Lu, M. A. Kelly, W. You and L. Yu, *Nat. Photonics*, 2015, **9**, 491.
135 B. M. Savoie, S. Dunaisky, T. J. Marks and M. A. Ratner, *Adv. Energy Mater.*, 2014, **5**, 1400891.
136 T. Ameri, P. Khoram, J. Min and C. J. Brabec, *Adv. Mater.*, 2013, **25**, 4245.
137 L. Yang, L. Yan and W. You, *J. Phys. Chem. Lett.*, 2013, **4**, 1802.
138 Y. C. Chen, C. Y. Hsu, R. Y. Y. Lin, K. C. Ho and J. T. Lin, *ChemSusChem*, 2013, **6**, 20.
139 P. P. Khlyabich, B. Burkhart, A. E. Rudenko and B. C. Thompson, *Polymer*, 2013, **54**, 5267.
140 Y. J. Hwang, B. A. E. Courtright and S. A. Jenekhe, *MRS Commun.*, 2015, **5**, 229.
141 H. Benten, T. Nishida, D. Mori, H. Xu, H. Ohkita and S. Ito, *Energy Environ. Sci.*, 2016, **9**, 135.
142 D. Bartesaghi, I. d. C. Pérez, J. Kniepert, S. Roland, M. Turbiez, D. Neher and L. J. A. Koster, *Nat. Commun.*, 2015, **6**, 7083.
143 J. A. Bartelt, D. Lam, T. M. Burke, S. M. Sweetnam and M. D. McGehee, *Adv. Energy Mater.*, 2015, **5**, 1500577.